Pacific Northwest
NATIONAL LABORATORY

PNNL-35884, Rev. 1
EWG-RPT-046, Rev. 1

Glass Property-Composition Models Update for use in Direct Feed High-Level Waste Flowsheet Development

August 2025

John D Vienna
Xiaonan Lu
Pavel Ferkl
LaGrande L Gunnell
Alejandro Heredia-Langner
Nicholas A Lumetta
Tongan Jin
Joelle T Reiser
Vivianaluxa Gervasio

U.S. DEPARTMENT OF ENERGY

Prepared for the U.S. Department of Energy
under Contract DE-AC05-76RL01830

DISCLAIMER

PACIFIC NORTHWEST NATIONAL LABORATORY
operated by
BATTELLE
for the
UNITED STATES DEPARTMENT OF ENERGY
under Contract DE-AC05-76RL01830

Printed in the United States of America

Available to DOE and DOE contractors from
the Office of Scientific and Technical Information,
P.O. Box 62, Oak Ridge, TN 37831-0062
www.osti.gov
ph: (865) 576-8401
fox: (865) 576-5728
email: reports@osti.gov

Available to the public from the National Technical Information Service
5301 Shawnee Rd., Alexandria, VA 22312
ph: (800) 553-NTIS (6847)
or (703) 605-6000
email: info@ntis.gov
Online ordering: http://www.ntis.gov

PNNL-35884, Rev. 1
EWG-RPT-046, Rev. 1

Glass Property-Composition Models Update for use in Direct Feed High-Level Waste Flowsheet Development

August 2025

John D Vienna
Xiaonan Lu
Pavel Ferkl
LaGrande L Gunnell
Alejandro Heredia-Langner
Nicholas A Lumetta
Tongan Jin
Joelle T Reiser
Vivianaluxa Gervasio

Prepared for
the U.S. Department of Energy
under Contract DE-AC05-76RL01830

Pacific Northwest National Laboratory
Richland, Washington 99354

Change History

Revision	Date Issued	Description of Change
0	May 2024	Initial Issue.
1	August 2025	Page 33, table 3-1, CI values for sulfate, K-3 corrosion and phosphate models were changed from 90% to 95%. Page 34, note [8] for table 3-1. One sentence was added at the end to clarify the model prediction uncertainty calculation, which is “PCT, sulfate, K-3 corrosion and phosphate and 1-sided intervals while viscosity and conductivity are 2-sided.”

Abstract

A set of preliminary glass property models and constraints were developed and augmented by models from literature for use in design of direct-feed high-level waste (DFHLW) glasses for flowsheet evaluation, testing, and design of the Tank Waste Treatment and Immobilization Plant (WTP) high-level waste (HLW) Facility. These models and constraints are meant to be used as a place-holder while glass property-composition data gaps are filled and final plant operating models are developed. This report describes the motivation and intended use of the models, the compilation of data, model fitting and selection, methods to apply the models and constraints in glass design and offers example calculations demonstrating their intended use.

Quality Assurance

This work was performed in accordance with the PNNL Nuclear Quality Assurance Program (NQAP). The NQAP complies with DOE Order 414.1D, *Quality Assurance*, and 10 CFR 830, *Nuclear Safety Management*, Subpart A, *Quality Assurance Requirements*. The NQAP uses NQA-1-2012, *Quality Assurance Requirements for Nuclear Facility Application*, as its consensus standard and NQA-1-2012, Subpart 4.2.1, as the basis for its graded approach to quality.

The NQAP works in conjunction with PNNL's laboratory-level Quality Management Program, which is based on the requirements as defined in DOE Order 414.1D and 10 CFR 830 Subpart A.

The work of this report was performed to a technology readiness level of 6.

Acknowledgments

The authors gratefully acknowledge the financial support provided by the U.S. Department of Energy Office of River Protection Waste Treatment and Immobilization Plant Project, with technical oversight by Albert Kruger. The following Pacific Northwest National Laboratory staff members are acknowledged for their contributions: Jarrod Crum for technical review of the report, David MacPherson for quality assurance, Chrissy Charron, and Cassie Martin for programmatic support during the conduct of this work, Renee Russell and Will Eaton for project management. We thank Bob Hanson, Shea Voss, John Julyk, Malinda Ham, Steve Barnes, and Bharthwaj Anantharaman from Bechtel National Inc. for motivation and helpful discussions.

Acronyms and Other Abbreviations

3TS	three times saturation (method)
Alt-18	(Analysis of Alternatives) alternative #18
APPS	Aspen Process Performance Simulation (WTP steady-state flowsheet model)
BOF	balance of facilities
CaxP	$CaO \times P_2O_5$
CCC	canister centerline cooling
CI	confidence interval
DFHLW	Direct-Feed High-Level Waste
DOE	U.S. Department of Energy
DWPF	Defense Waste Processing Facility
EC	electrical conductivity
EWG	enhanced waste glass
EWG2	second iteration of enhanced waste glass
FIO	For Information Only
GFC	glass-forming chemical
HLW	high-level waste (Facility)
LAB	WTP Laboratory
LAW	low-activity waste (Facility)
MV	model validity
NL	normalized loss by 7-day PCT
NQAP	Nuclear Quality Assurance Program
ORP	Office of River Protection
PCT	Product Consistency Test
PNNL	Pacific Northwest National Laboratory
PT	Pretreatment (Facility)
RMSE	root mean squared error
SUCI	simultaneous upper confidence interval
TCLP	toxicity characteristic leaching procedure
TOC	total organic carbon
TSCR	Tank Side Cesium Removal (system)
V	viscosity
VFT	Vogel-Fulcher-Tammann (viscosity-temperature equation)
WL	waste loading
wt%	weight percent
WTP	Waste Treatment and Immobilization Plant
XRD	X-ray diffraction

Symbols

A	preexponential term in VFT viscosity- or EC-temperature equation
B	temperature effect term in VFT viscosity- or EC-temperature equation
B_i	temperature effect coefficient for i^{th} component viscosity or EC model
c_α	concentration of element α in PCT test solution (α = B, Na, Li)
f_α	concentration of element α in glass (α = B, Na, Li)
g_i	mass fraction of i^{th} component in glass
k_{1208}	K-3 refractory neck corrosion at 1208 °C
k_{bubb}	K-3 refractory neck corrosion at 1208 °C using bubbled method
k_i	ith component coefficient for K-3 refractory neck corrosion model
k_s	an offset for k_{stat} data compared to k_{bubb} data
k_{stat}	K-3 refractory neck corrosion at 1208 °C using static method
n	number of datapoints used to fit a model
N_{ALK}	normalized alkali content in glass
N_{NaLi}	normalized soda and lithia content in glass
N_{SiAl}	normalized silica-alumina content in glass
NL_α	normalized loss of component α during 7-day PCT (α = B, Na, Li)
p	probability of nepheline formation
p	number terms in a model
p_i	i^{th} component model coefficient
p_{ii}	i^{th} component quadratic term model coefficient
p_{ij}	i^{th} and j^{th} components cross-product term model coefficient
q	number of normalized PCT responses for a given glass
S	glass surface area in PCT test
$S_{0/1}$	a static method counter (= 1 for k_{stat}, = 0 for k_{bubb})
T	temperature
T_0	infinite viscosity or EC temperature value in VFT equation
$T_{2\%}$	temperature at 2 vol% spinel
T_M	melting temperature
T_L	liquidus temperature
T_L-Zr	liquidus temperature for zirconium-containing phases
U_{pred}	prediction uncertainty
V	PCT solution volume
w_i	ith component w_{SO3} model coefficient
wt%	weight percent
w_{SO3}	sulfur solubility
$w_{SO3\text{-}MT}$	sulfur solubility by melter tolerance method

$w_{SO3\text{-}bub}$	sulfur solubility by bubbling method
$w_{SO3\text{-}sat}$	sulfur solubility by saturation method
$w_{SO3\text{-}3TS}$	sulfur solubility by three times saturation method
x_i	normalized concentration of *i*th component in glass
ε	electrical conductivity
ε_{1100}	electrical conductivity at 1100 °C
ε_{1150}	electrical conductivity at 1150 °C
ε_{1200}	electrical conductivity at 1200 °C
η_{1100}	viscosity at 1100 °C
η_{1150}	viscosity at 1150 °C
η_T	viscosity at temperature, T
ρ	density

Contents

Figures

Tables

1.0 Introduction

The U.S. Department of Energy (DOE) Office of River Protection (ORP) is responsible for the safe storage, treatment, and immobilization of wastes stored in underground tanks at the Hanford Site. The Waste Treatment and Immobilization Plant (WTP) is the cornerstone of tank waste treatment and immobilization strategy at Hanford. This plant includes, as primary components, the Low-Activity Waste (LAW) Facility, the High-Level Waste (HLW) Facility, the Pretreatment (PT) Facility, the Laboratory (LAB), and the balance of facilities (BOF). The current strategy is to stage the startup of the LAW, HLW, and PT facilities (DOE 2013; Bernards et al. 2020). The startup of the LAW Facility along with the needed components of the LAB and the BOF are planned for 2024. To facilitate the startup of the LAW Facility prior to the PT Facility, a Tank Side Cesium Removal (TSCR) system was constructed to remove solids and cesium-137 (^{137}Cs) from the tank waste supernate, thereby sufficiently removing much of the radioactivity of the supernatant liquid to feed the LAW Facility (Westesen et al. 2022). The TSCR began operations on January 26, 2022.

An analysis of alternatives for startup and operations of the PT and HLW facilities was conducted to identify the most likely alternatives along with the upper-level implication of each (Parsons 2023). Seventeen options were considered, including concurrent startup of the HLW and PT facilities and HLW Facility operations without the PT Facility. Based on the results of these options, ORP requested an 18th scenario (alternative 18 or Alt-18) in which the annual budget for Hanford was constrained (Bernards et al. 2021). This scenario includes a Waste Transfer Vault that couples the HLW Facility with tank farms using a waste feed transfer vessel and an effluent collection vessel. ORP empaneled a group of technical experts from ORP, Bechtel National Inc. (the WTP contractor), Washington River Protections Solutions (the tank farm operations contractor), and Pacific Northwest National Laboratory (PNNL) to develop a flowsheet that could efficiently operate the HLW Facility for a ~12-year period under a Direct Feed High-Level Waste (DFHLW) flowsheet while the HLW Pretreatment and Effluent Management Facility is brought on-line. The general operating strategy laid out in Alt-18 was to serve as the reference case for DFHLW flowsheet development. Through this effort, the team identified the need to formulate glass using the enhanced waste glass (EWG) method, which results in reasonable waste processing rates (Vienna et al. 2023).

To complete the final design of the HLW Facility, complete flowsheet assessments are required. These assessments include mass, energy, and heat balances through the unit operations of the plant. The Aspen Process Performance Simulation (APPS) tool is used to perform the flowsheet calculations (Gebhardt 2011). Thirty-one APPS runs were performed in support of the baseline HLW flowsheet in the Process Inputs Basis of Design for HLW (Dunst 2020). The APPS software automatically generates a glass formulation based loosely on the WTP baseline glass formulation method (Vienna and Kim 2014). To enable the use of EWG formulations, the glass formulation method in APPS can be updated to include EWG formulation method or overridden with predetermined glass formulations. To support these options, glasses were formulated, fabricated, and tested using the EWG approach. The glass compositions and testing results are reported by Gervasio et al. (2024). The results suggested the need to update some glass property models as summarized in Table 1-1.

Table 1-1. Summary of Property Model Comparisons

Property	Disposition
CCC crystallinity	Both Lu et al. (2021) and Vienna et al. (2016) nepheline precipitation models predicted that no nepheline would form in any of the glasses from this study. However, glasses APPS-05 and -06 both precipitated nepheline on canister centerline cooling (CCC) and the resulting samples failed Product Consistency Test (PCT) constraints. It was recommended that more conservative predictions be used to control nepheline in DFHLW glasses.
Isothermal crystallinity	Zirconia-containing phases liquidus temperature (T_L) and spinel 2 volume percent crystal temperature ($T_{2\%}$) models from Vienna et al. (2016) successfully limited unacceptably high concentrations of these crystals (either the conservative 1 vol% or the more optimal 2 vol%) at 950 °C. However, glass APPS-05 precipitated 1.9 vol% $NaCaPO_4$ and 0.2 vol% Cr_2O_3 at 950 °C and glass APPS-07-2 precipitated 1.2 vol% $Na_3Nd(PO_4)_2$ and 0.6 vol% $Ca_2Fe_2O_5$ at 950 °C. Additional constraints are needed to control the formation of these phases for which models don't currently exist.
Sulfur solubility	Previous models significantly underpredicted the measured sulfur solubility (w_{SO3}) values. A new model for w_{SO3} using only the three-times-saturation method (3TS) data was developed which adequately predicts measured values ($w_{SO3\text{-}3TS}$).
Density	Densities (ρ) of APPS glasses are over-predicted by models from Vienna et al. (2002 and 2009). The Vienna (2002) model with a -0.03719 g/cm^3 offset adequately predicts density of APPS glasses.
Viscosity	Viscosities (η) of APPS glasses are not adequately predicted by models evaluated in this study. Updated models are needed to predict viscosities of DFHLW glasses.
Electrical conductivity	Electrical conductivity (EC) of APPS glasses are not adequately predicted by models evaluated in this study. Updated models are needed to predict EC of DFHLW glasses.
Product consistency test	PCT data are underpredicted by models evaluated in this study. Updated models are needed to predict PCT of DFHLW glasses.
Toxicity	Toxicity Characteristic Leaching Procedure (TCLP) values are slightly overpredicted by the Kim et al. (2003) model which will be used to predict TCLP responses of DFHLW glasses.
K-3 neck corrosion	K-3 neck corrosion (k_{1208}) data are underpredicted by the models evaluated. Updated models are needed to predict K-3 corrosion of DFHLW glasses.

Each of these model updates are discussed in this report. PCT models are summarized in Section 2.1, η and EC models are summarized in Section 2.2, w_{SO3} model is summarized in Section 2.3, k_{1208} model is summarized in Section 2.4, and phosphate crystal constraint (Phos) is summarized in Section 2.5. Glass formulation constraints and methods are discussed in Section 3.0.

2.0 Property Models

2.1 Product Consistency Test Response

PCT responses are measured for boron, sodium, and lithium concentrations (c_α for α = B, Na, and Li) in solution after the 7-day, 90 °C test. The concentrations are normalized for both the concentration of those components in the glass (f_α) and the estimated glass surface area to solution volume (S/V = 2000 m^{-1}). The normalized losses (NL_α) are given by: $NL_\alpha = \frac{c_\alpha}{f_\alpha S/V}$. If the glass alters congruently, then $NL_B = NL_{Na} = NL_{Li}$ which translates to the mass of glass dissolved per surface area.

The APPS glass PCT data were compared to models for both LAW and HLW models and neither predicted PCT for most APPS glasses well. The lower Na_2O glasses were reasonably well predicted by the HLW model from Vienna and Crum (2018).

2.1.1 Database

The composition region of primary interest is HLW with high LAW concentrations. So, it was decided to fit a new model to combined LAW glass data and the APPS DFHLW glass data (Gervasio et al. 2024).

For LAW glasses, NL_{Na} and NL_B are constrained and so LAW glass PCT data generally only tabulate and track NL_{Na} and NL_B. For HLW glasses, the NL_B, NL_{Na}, NL_{Li} are all constrained. To simplify the model development and implementation, the average ln[NL_α] were calculated according to: $Ave\ln[NL] = \sum_{\alpha=B,Na,Li}^{q} \ln[NL_\alpha]/q$, where q is the number of results for any given glass. First, the NL_α were plotted versus each other to determine if outliers existed. Nine values were not included in the averaging: LP5-04 NL_B, LAW-HPVR-18 NL_{Na}, LAW-HPVR-20 NL_B and NL_{Na}, APPS-04 NL_B, APPS-05 NL_{Na}, APPS-06 NL_{Na}, APPS-09 NL_B, and APPS-13 NL_B. This left 221 glasses with Ave ln[NL] for fitting. The range of data are summarized in Table 2-1. A significant negative correlation between the concentrations of Na_2O and Li_2O (-0.7352) was observed, so the range of $N_{ALK} = g_{Na2O} + 0.66\ g_{K2O} + 2.07\ g_{Li2O}$ must also be maintained.

Table 2-1. Validity range for PCT Ave ln[NL] model

Component	Min	Median	Max
Al_2O_3	0.030007	0.063323	0.263214
B_2O_3	0.04001	0.095329	0.221695
CaO	0	0.068309	0.12919
Cl	0.000482	0.00284	0.024101
Cr_2O_3	0.000101	0.002128	0.014357
F	0.00036	0.002147	0.045162
Fe_2O_3	0	0.004832	0.068502
K_2O	0	0.01005	0.058434
Li_2O	0	0	0.051217
MgO	0	0.003418	0.050555

Component	Min	Median	Max
Na_2O	0.092261	0.212365	0.270387
P_2O_5	0.000672	0.005641	0.03987
SO_3	0.00036	0.00664	0.0177
SiO_2	0.247553	0.392284	0.584707
SnO_2	0	0.01611	0.050757
TiO_2	0	0	0.029392
V_2O_5	0	0.018517	0.057301
ZnO	0	0.02002	0.057517
ZrO_2	0	0.033384	0.092735
Others	0	0	0.034793
AveLn[*NL*, g/m^2]	-1.89241	0.009901	3.695903
N_{ALK}	0.128529	0.242585	0.300954

2.1.2 Model

A model was developed to predict the Ave ln[*NL*] data described in Section 2.1.1. The distribution of each composition term was evaluated in 1-dimension using histogram plots and 2-dimensions using scatterplot matrices to determine which terms had sufficient range and variation to be used in modeling. The following 19 oxides and halogens were found to be appropriate potential model terms: Al_2O_3, B_2O_3, CaO, Cl, Cr_2O_3, F, Fe_2O_3, K_2O, Li_2O, MgO, Na_2O, P_2O_5, SiO_2, SO_3, SnO_2, TiO_2, V_2O_5, ZnO, and ZrO_2.

A first-order composition model of the form: $Ave\ln[NL]=\sum_{i=1}^{n}p_i g_i$, where p_i and g_i are the i^{th} component coefficient and mass fraction, respectively.

It was found that Al_2O_3, B_2O_3, CaO, Li_2O, Na_2O, SiO_2, SnO_2, TiO_2, V_2O_5, ZnO, and ZrO_2 were found to be statistically significant. Two datapoints, LP5-02 and LAWALG-03, were found to be fit outliers with studentized residuals > 3 so were excluded from the fit. The addition of cross-product or quadratic terms were then investigated to determine if a small number of higher order terms would significantly improve the model performance using:

$$Ave\ln[NL]=\sum_{i=1}^{n}p_i g_i+Selected\left\{\sum_{i=1}^{n}p_{ii}g_i^2+\sum_{i=1}^{n}\sum_{j\neq i}^{n-1}p_{ij}g_i g_j\right\}$$, where p_{ii} is the i^{th} component quadratic coefficient and p_{ij} is the i^{th}-j^{th} cross product coefficient. It was found that the addition of two second order terms: $Al_2O_3 \times Al_2O_3$ and $Al_2O_3 \times CaO$ significantly improved the model fit. Adding these two terms increases the R^2 from 0.7769 for the first order model to 0.8251. The third most significant second order term $Al_2O_3 \times TiO_2$ increased the R^2 to 0.8262. Clearly the third term gives diminishing returns.

Model coefficients and summary statistics are given in Table 2-2. The predicted versus measured plots are shown in Figure 2-1, and composition effects on Ave ln[*NL*] are shown graphically in Figure 2-2.

Table 2-2. Product consistency test Ave ln[*NL*, g/m^2] model coefficients and summary statistics, composition in mass fractions

Term	Estimate	Statistic	Value
Al_2O_3	-53.15774	# of points, n	219
B_2O_3	12.07217	# of terms, p	13
CaO	-14.77972	Mean	0.2584
Li_2O	29.306445	R^2_{fit}	0.8251
Na_2O	18.110349	R^2_{press}	0.7958
SiO_2	-4.531755	$RMSE_{fit}$	0.5073
SnO_2	-10.12384	$RMSE_{press}$	0.5328
V_2O_5	5.2426736		
ZnO	-12.22331		
ZrO_2	-1.421716		
Others	12.938447		
Al_2O_3×Al_2O_3	137.13002		
Al_2O_3×CaO	117.30595		

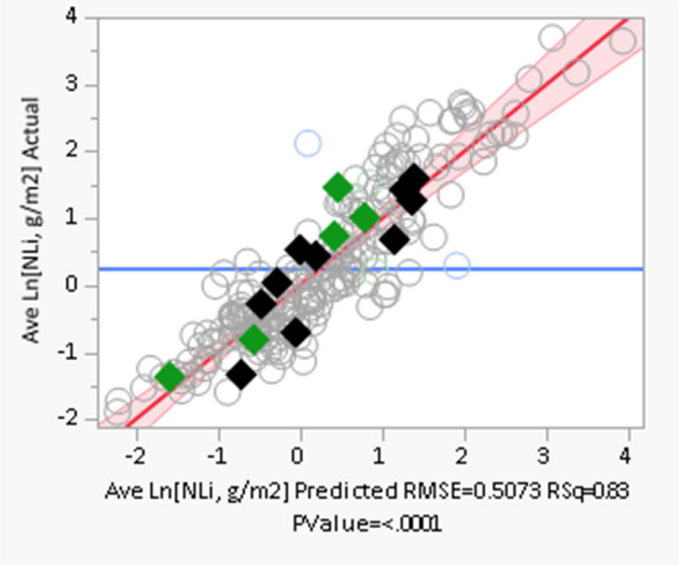

Figure 2-1. Predicted versus measured Ave ln[*NL*, g/m^2]. Solid diamonds represent APPS glasses, blue circles represent outliers that have been removed from the fit, blue line indicates the mean measured value.

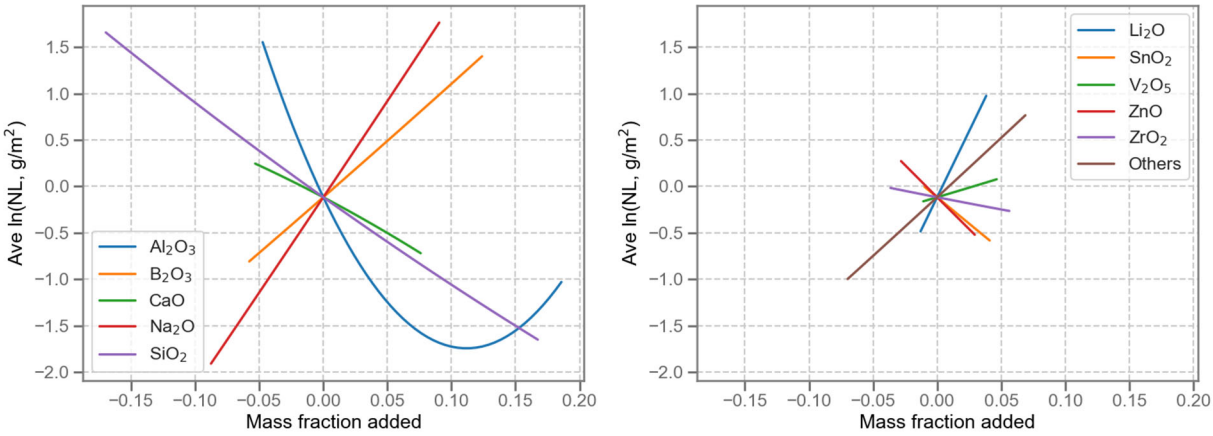

Figure 2-2. Component effects on Ave ln[*NL*, g/m^2] (For Information Only).

2.2 Viscosity and Electrical Conductivity

The constraints on glass melt η and EC, ε, are set to provide sufficient processability while limiting refractory corrosion and current density near electrodes. Both properties are affected by temperature and glass composition. Neither HLW nor LAW models could satisfactorily estimate the measured viscosity or electrical conductivity of APPS glasses (Gervasio et al. 2024). Thus, updated models were formulated.

2.2.1 Database

The models were developed using data for LAW (Vienna et al. 2022) and APPS (Gervasio et al. 2024) glasses. Thus, the database consisted of 4,487 η points for 654 glasses and 4,462 EC points for 643 glasses. For both properties, 80 % of glasses were randomly selected for model training and the remaining 20 % were left for model testing. Figure 2-3 shows that for a given temperature, the measured values of η and ε of APPS glasses are mostly aligned with the LAW dataset. However, compared to the LAW dataset, APPS glasses have larger composition variations in SiO_2, B_2O_3, Al_2O_3, and F and smaller composition variations in ZnO, Fe_2O_3, MgO, K_2O, and SnO_2 (Figure 2-4).

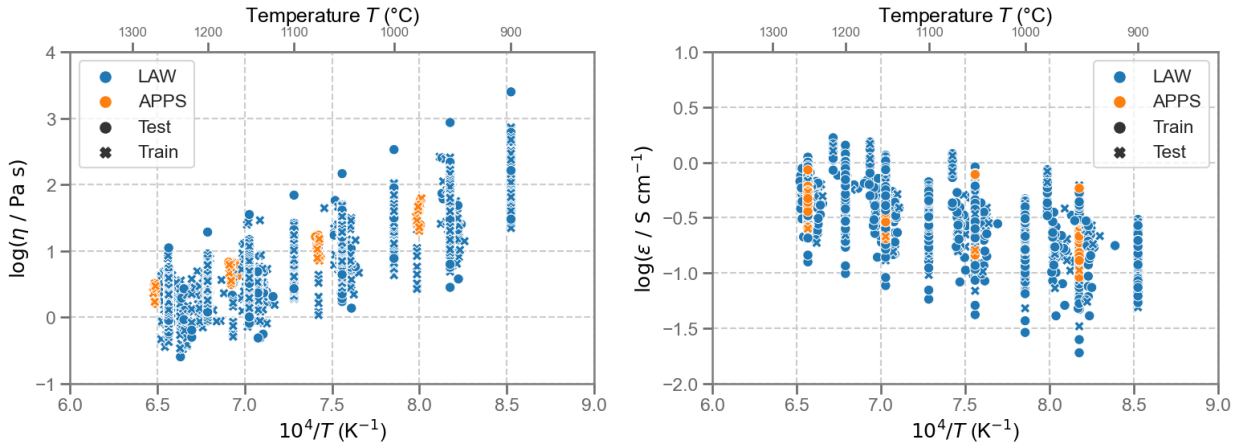

a) Viscosity b) Electrical conductivity

Figure 2-3. Measured a) viscosity and b) electrical conductivity versus inverse temperature.

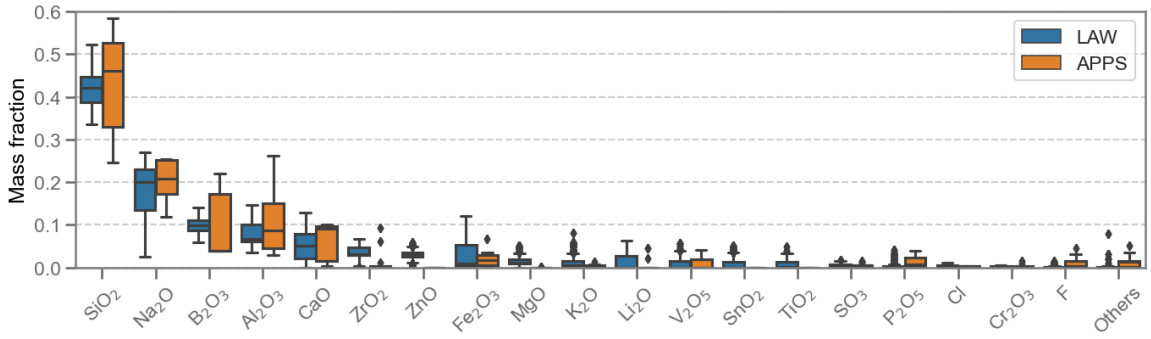

Figure 2-4. Box plot showing minimum, median, and maximum component mass fractions in glass for LAW and APPS data.

2.2.2 Model

The temperature- and composition-dependence of viscosity and electrical conductivity was modeled using the Vogel-Fulcher-Tammann (VFT) equation, which can be written as:

$$\log10(\eta) = A + \frac{B}{T - T_0}$$

where $\log(\eta)$ is a decadic logarithm of viscosity (replaced by $\log(\varepsilon)$ for electrical conductivity), and A, B, and T_0 are parameters of the VFT equation. Parameters A, and T_0 were modeled as constants while a linear model was used for the activation energy parameter as

$$B = \sum_{i=1}^{N} g_i B_i$$

where N is the number of components, g_i is the *i*th component mass fraction, and B_i is the *i*th component coefficient. The following components were chosen as model terms: Al_2O_3, B_2O_3, CaO, Fe_2O_3, K_2O, Li_2O, MgO, Na_2O, P_2O_5, SiO_2, SnO_2, TiO_2, V_2O_5, ZnO, ZrO_2, and Others. Thus, the models contain 18 coefficients fitted by the least squares method.

Figure 2-5 shows the measured versus estimated viscosity and electrical conductivity for both LAW and APPS glasses. There are no obvious outliers in APPS data, but the model has a slight tendency to overestimate the electrical conductivity of APPS glasses and the mean estimate errors are larger for APPS glasses for both viscosity and electrical conductivity (see Table 2-3). Model parameters are listed in Table 2-4.

Composition effects on a centroid reference glass are shown graphically in Figure 2-6 (η) and Figure 2-7 (ε). These effects are consistent with previously measured component effects (e.g., Vienna et al. (2022) and Heredia-Langner et al. (2022)).

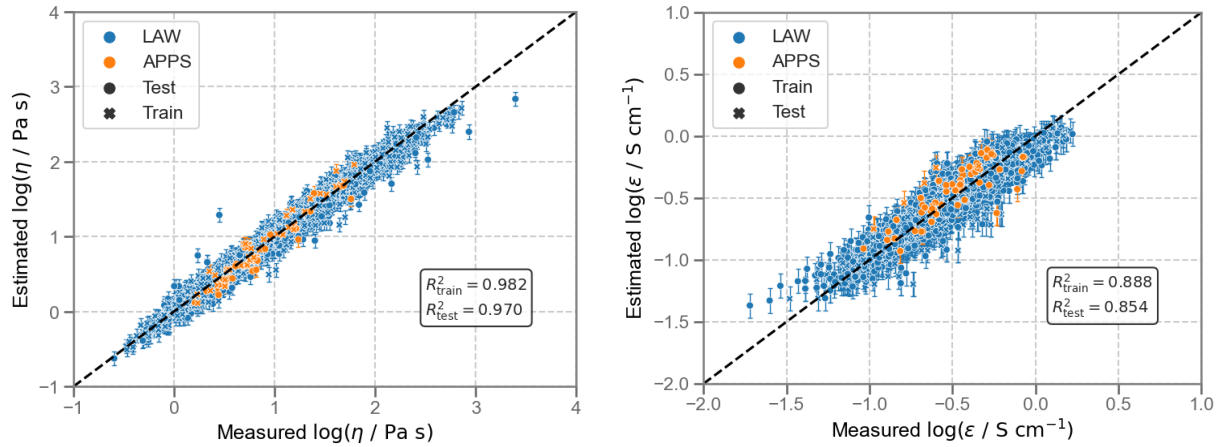

a) Viscosity b) Electrical conductivity

Figure 2-5. Measured versus estimated a) viscosity and b) electrical conductivity. The notches display the 90 % prediction intervals.

Table 2-3. Metrics of viscosity (V) and electrical conductivity (EC) models.

Set	Type	R^2, V	R^2, EC	RMSE, V	RMSE, EC
Test	APPS	0.855	0.245	0.152	0.193
Test	LAW	0.971	0.859	0.104	0.097
Train	APPS	0.929	0.637	0.104	0.126
Train	LAW	0.982	0.892	0.080	0.083

Table 2-4. Viscosity and EC model parameters.

Set	η	ε
A (log(Pa s))	-2.6135	0.772566
*B*_Al_2O_3 (K^{-1})	6632.044	-2087.53
*B*_B_2O_3 (K^{-1})	-519.437	-1414.09
*B*_CaO (K^{-1})	-389.161	-1842.64
*B*_Fe_2O_3 (K^{-1})	1642.818	-1266.8
*B*_K_2O (K^{-1})	623.434	-641.96
*B*_Li_2O (K^{-1})	-10199.1	4635.015
*B*_MgO (K^{-1})	2055.801	-1003.17
*B*_Na_2O (K^{-1})	-1311.46	1980.649
*B*_P_2O_5 (K^{-1})	3729.876	-2337.66
*B*_SiO_2 (K^{-1})	5257.354	-1834.85
*B*_SnO_2 (K^{-1})	3757.721	-2442.23
*B*_TiO_2 (K^{-1})	1644.819	-1087.99
*B*_V_2O_5 (K^{-1})	1022.555	-672.313
*B*_ZnO (K^{-1})	929.4394	-731.135
*B*_ZrO_2 (K^{-1})	4921.279	-1831.21
*B*_Others (K^{-1})	1907.84	-713.126
T_0 (K)	600.804	600.9442

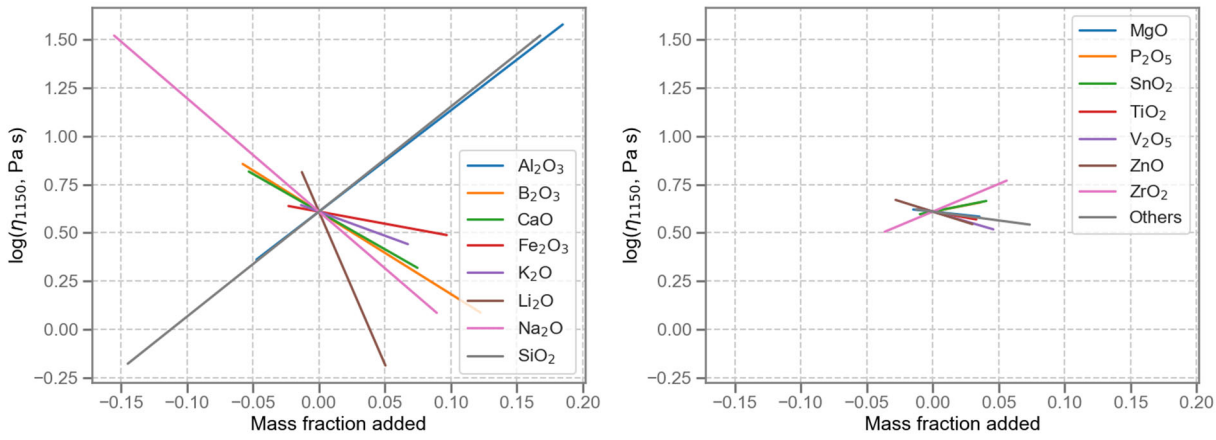

Figure 2-6. Component effect on log(η_{1150}, Pa·s) (For Information Only).

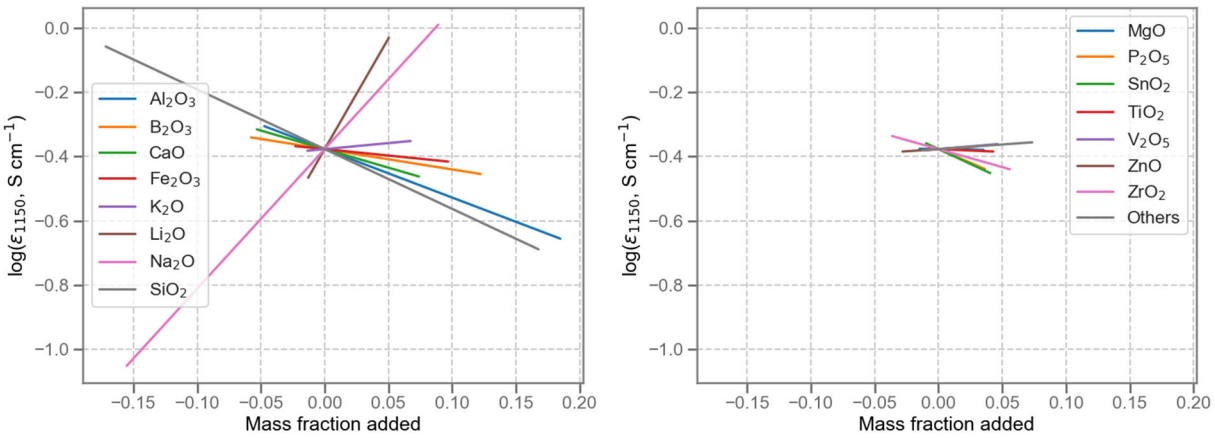

Figure 2-7. Component effect on log(ε_{1150}, S/cm) (For Information Only).

2.3 Melter SO_3 Tolerance

The measured w_{SO3} of APPS glasses were poorly predicted by existing models including those from Vienna et al. (2013, 2014, 2016, 2022) and Muller et al. (2018). The predicted w_{SO3} values were grossly underpredicted for most models for all APPS data (after accounting for offsets between measurement methods). The exception being the Vienna et al. (2014) model which predicted close to the measured values for $w_{SO3} \leq 1.7$ wt% and under predicted all $w_{SO3} > 1.7$ wt%. Therefore, a new model was deemed appropriate.

The most appropriate sulfur-related constraint for use in glass design is the melter tolerance value that is measured by systematically increasing the concentration of SO_3 in the melter feed until the feed processed at steady-state is observed to accumulate a molten salt layer. This data is referred to as $w_{SO3\text{-}MT}$ for melter tolerance. This method requires the use of scaled melter tests which are time-consuming and expensive. As a result, only 13 $w_{SO3\text{-}MT}$ data are available. Crucible scale tests have been systematically performed on Hanford waste glasses using three different test methods: (1) bubbling ($w_{SO3\text{-}bub}$) where a mixture of O_2 and SO_2 gasses are bubbled through the glass melt until the melt is supersaturated with SO_3; (2) saturation ($w_{SO3\text{-}sat}$) where glass is melted with an excess of Na_2SO_4 and the concentration of SO_3 is measured after removing the excess salt; (3) three-times saturation ($w_{SO3\text{-}3TS}$) is similar to $w_{SO3\text{-}sat}$ except the melt is ground and remelted to supersaturate the melt three consecutive times before removing the salt and analyzing the SO_3. These methods are more fully described and compared by Skidmore et al. (2019). It was found that the $w_{SO3\text{-}3TS}$ method results in measured SO_3 values that correlate to the $w_{SO3\text{-}MT}$ value with the smallest uncertainty as shown in Figure 2-8. The $w_{SO3\text{-}3TS}$ results average 0.33 wt% below the $w_{SO3\text{-}MT}$ for the 13 glasses tested for melter tolerance. Combining data from multiple test methods results in higher prediction uncertainty, a broader difference between crucible data and MT data, and significant underpredictions at higher w_{SO3} values (Vienna et al. 2022). Therefore, it was decided to model the $w_{SO3\text{-}3TS}$ data only as a function of composition.

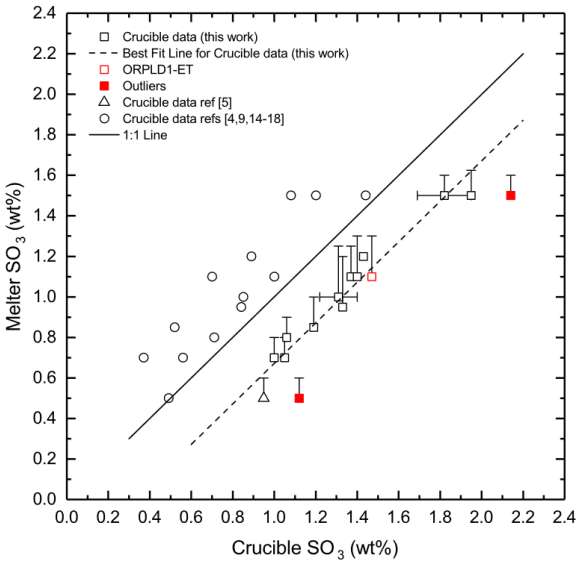

Figure 2-8. Comparison of $w_{SO3\text{-}MT}$ with crucible methods, from Skidmore et al. (2019).

2.3.1 Database

The available $w_{SO3\text{-}3TS}$ data is primarily for Hanford LAW glasses. The data was compiled from 225 glasses gathered from 10 studies as summarized in Table 2-5. The ranges of measured $w_{SO3\text{-}3TS}$ values and component concentrations are listed in Table 2-6.

Table 2-5. Summary of $w_{SO3\text{-}3TS}$ model data

Study	# of $w_{SO3\text{-}3TS}$ points	Reference
LAW-Ph1	34	Russell et al. (2017)
LAW-Ph2	41	Russell et al. (2021)
LAW-Ph3	23	Lonergan et al. (2019)
LAW-Ph4	25	Gervasio et al. (2021)
LAW-Ph5	25	Gervasio et al. (2023)
HPVR	26	Gervasio et al. (2023)
EMHQ-LBE	12	Russell et al. (2022)
LAWALG	17	Gervasio et al. (2022)
LAWML1	7	Lu et al. (2024)
DFHLW APPS	15	Gervasio et al. (2024)
Total	225	

Table 2-6. Range of $w_{SO3\text{-}3TS}$ data used in model development, normalized mass fraction

Component	Min	Median	Max
Al_2O_3	0.0305	0.0633	0.2639
B_2O_3	0.0402	0.0953	0.2228
CaO	0.0000	0.0696	0.1292
Cl	0.0005	0.0028	0.0241
Cr_2O_3	0.0001	0.0021	0.0144
F	0.0004	0.0021	0.0453
Fe_2O_3	0.0000	0.0048	0.0689
K_2O	0.0000	0.0101	0.0584
Li_2O	0.0000	0.0000	0.0512
MgO	0.0000	0.0034	0.0506
Na_2O	0.0923	0.2124	0.2704
P_2O_5	0.0007	0.0056	0.0403
SiO_2	0.2488	0.3923	0.5936
SnO_2	0.0000	0.0161	0.0508
TiO_2	0.0000	0.0000	0.0294
V_2O_5	0.0000	0.0189	0.0573
ZnO	0.0000	0.0200	0.0575
ZrO_2	0.0000	0.0334	0.0930
Others	0.0000	0.0000	0.0351
$w_{SO3\text{-}3TS}$, wt%	0.602	1.54	3.13

2.3.2 Model

A model was developed to predict the $w_{SO3\text{-}3TS}$ data described in Section 2.3.1. The distribution of each composition term was evaluated in 1-dimension using histogram plots and 2-dimensions using scatterplot matrices to determine which terms had sufficient range and variation to be used in modeling. The following 18 oxides and halogens were found to be appropriate potential model terms: Al_2O_3, B_2O_3, CaO, Cl, Cr_2O_3, F, Fe_2O_3, K_2O, Li_2O, MgO, Na_2O, P_2O_5, SiO_2, SnO_2, TiO_2, V_2O_5, ZnO, and ZrO_2.

A first-order composition model of the form: $w_{SO_3-3TS} = \sum_{i=1}^{n} w_i x_i$, where w_i and x_i are the i^{th} component coefficient and normalized mass fraction, respectively; where $x_i = g_i/(1-g_{SO3})$.

It was found that B_2O_3, CaO, F, K_2O, Li_2O, Na_2O, P_2O_5, SiO_2, TiO_2, V_2O_5, and ZrO_2 were statistically significant. This first-order model resulted in an $R^2 = 0.7834$ and an RMSE = 0.2276 wt%. The addition of cross-product or quadratic terms were then investigated to determine if a small number of higher order terms would significantly improve the model performance using:

$$w_{SO_3-3TS} = \sum_{i=1}^{n} w_i x_i + Selected\left\{\sum_{i=1}^{n} w_{ii} x_i^2 + \sum_{i=1}^{n}\sum_{j\neq i}^{n-1} w_{ij} x_i x_j\right\}$$

, where w_{ii} is the i^{th} component quadratic coefficient and w_{ij} is the i^{th}-j^{th} cross product coefficient. It was found that the addition CaO×SiO_2, Al_2O_3×Na_2O, and B_2O_3×CaO significantly improved the model fit. With the three cross product terms, the first order term for Al_2O_3 was added and the term from TiO_2 was found to be insignificant. The partial quadratic mixture (PQM) model has an $R^2 = 0.8363$ and an RMSE = 0.1993 wt%.

Coefficients for the two models are given in Table 2-7. The predicted versus measured plots are shown in Figure 2-9. These coefficients do not account for the -0.33 wt% offset between melter tolerance and 3TS. Therefore, users must adjust predicted $w_{SO3\text{-}3TS}$ values to estimate melter tolerance: $w_{SO_3-MT} = w_{SO_3-3TS} - 0.33$. Composition effects on $w_{SO3\text{-}3TS}$ are shown graphically in Figure 2-10.

Table 2-7. 3TS SO_3 solubility model coefficients and summary statistics, composition in normalized mass fractions and w_{SO3} in wt%

Term	1st Order	PQMM	Statistic	1st Order	PQMM
Al_2O_3	-	3.311369	# of points, n	225	225
B_2O_3	4.5692212	2.480127	# of terms, p	12	15
CaO	5.3841223	-19.2638	Mean	1.621	1.621
F	2.1977901	2.90893	R^2_{fit}	0.7834	0.8363
K_2O	2.2187806	3.564656	R^2_{press}	0.7550	0.8071
Li_2O	13.202296	15.83879	$RMSE_{fit}$	0.2276	0.1993
Na_2O	6.0284835	10.68731	$RMSE_{press}$	0.2361	0.2095
P_2O_5	1.8696893	4.275421			
SiO_2	0.4636885	-2.11066			
TiO_2	0.3669367	-			
V_2O_5	7.6672039	7.299997			

Term	1st Order	PQMM	Statistic	1st Order	PQMM
ZrO_2	-6.566486	-4.67831			
Others	-5.064627	-2.85583			
B_2O_3 x CaO	-	46.86848			
Al_2O_3 x Na_2O	-	-43.0749			
CaO x SiO_2	-	52.50427			

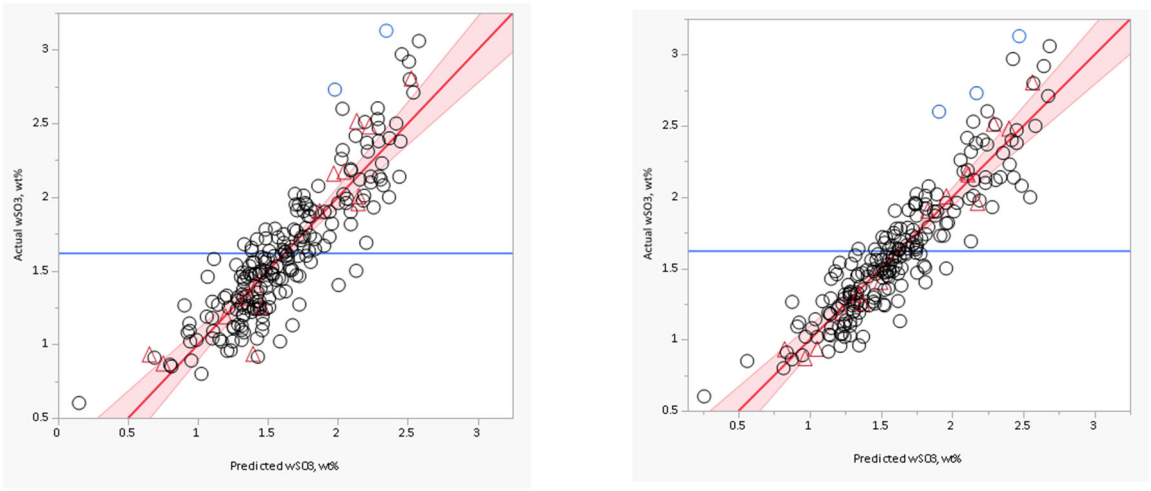

a) 1st Order Model b) PQMM

Figure 2-9. Predicted versus measured $w_{SO3\text{-}3TS}$ in wt%. Red triangles represent APPS glasses, blue circles represent potential outliers that have not been removed from the fit, blue line indicates the mean measured value.

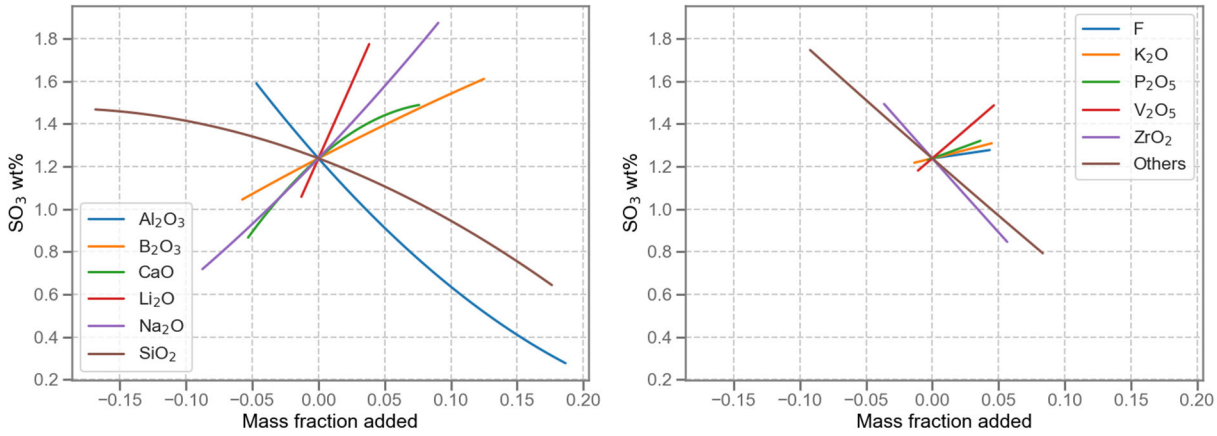

Figure 2-10. Component effects on $w_{SO3\text{-}3TS}$ (For Information Only).

2.4 K-3 Refractory Corrosion Neck Loss

Excessive corrosion of melter refractories has long been a concern for Hanford LAW glass design (Muller et al. 2018; and Vienna et al. 2013, 2016, 2022). However, typical Hanford HLW glass melts were not sufficiently corrosive to warrant concern for glass contact refractory corrosion. As higher concentrations of Hanford LAW components are likely to be in direct-feed wastes for Hanford HLW, K-3 refractory corrosion needs to be controlled as part of glass formulation.

K-3 corrosion data is relatively limited in both number of glasses and composition region covered (Vienna et al. 2022). The data that exists was measured for 6-days at 1208 °C. Most of that data was bubbled with air while a smaller dataset, including the DFHLW APPS glasses, was measured using a static test. In both cases, the refractory-air-melt triple point resulted in the highest corrosion. It is this neck region of corrosion that is used to model melt composition impact on K-3 corrosion. Bubbled tests result in broader but shallower corrosion at the neck compared to the static tests. The lack of data coverage by either test method necessitates the combination of data from the two methods to develop the broadest possible composition-K3 corrosion model.

2.4.1 Database

K-3 neck dimensional loss in inches (k_{1208}) data were compiled from both static (k_{stat}) and bubbled (k_{bubb}) corrosion test methods from two primary sources Muller et al. (2018) (344 k_{bubb}) and Amoroso et al. (2024) (15 k_{stat}). Four additional glasses previously tested using the bubbled method were retested using the static method to give a direct comparison. A total of 362 glasses were compiled. The distributions of component concentrations were evaluated using histograms for individual (1D) coverage and a scatterplot matrix for pair-wise (2D) coverage. As SO_3 and Cl partially volatilize during fabrication and volatilize significantly more (to an unknown extent) during corrosion measurement, they were removed from the glass composition and the remaining components were renormalized. The normalized mass fraction is expressed as $x_i = g_i/(1-g_{SO3} - g_{Cl})$. It was determined that Al_2O_3, B_2O_3, CaO, Cr_2O_3, F, Fe_2O_3, K_2O, Li_2O, MgO, MnO, Na_2O, NiO, P_2O_5, SiO_2, SnO_2, TiO_2, V_2O_5, ZnO, and ZrO_2 had sufficient coverage to justify inclusion in modeling as independent terms. None of the rare earth oxides had sufficient coverage individually, however combined rare earth oxides ($g_{RE_2O_3} = g_{Ce_2O_3} + g_{Gd_2O_3} + g_{La_2O_3} + g_{Nd_2O_3}$) did have sufficient coverage and therefore the combination was included as an independent term.

Four glasses were excluded from the data set due to extreme composition or extreme k_{1208} response values. LAWA64 contained > 7 wt% SrO and glasses LAWB67, LORPM11, and LORPM38 had k_{bubb} values of 0.001 in. The range of each component concentration, along with median value for the remaining 358 glass dataset, is given in Table 2-8. The dataset showed significant correlation between Na_2O and Li_2O concentrations (-0.9070) and between Al_2O_3 and SiO_2 (-0.7357). The concentration ranges of combined normalized components (where the coefficients represent the ratio of component molecular weights) were therefore considered: $N_{ALK} = x_{Na_2O} + 0.66x_{K_2O} + 2.07x_{Li_2O}$ ranged from 0.1381 to 0.2743 and $N_{SiAl} = x_{SiO_2} + 1.697x_{Al_2O_3}$ ranged from 0.4570 to 0.7236.

Table 2-8. Component concentration ranges in ln[k_{1208}] dataset, normalized mass fractions

Component	Min	Median	Max
Al_2O_3	0.030486	0.077271	0.264437
B_2O_3	0.040311	0.099826	0.223285
CaO	0	0.043232	0.124501
Cr_2O_3	0	0.00081	0.014452
F	0	0.000804	0.04535
Fe_2O_3	0	0.010146	0.136862
K_2O	0	0.005171	0.081318
Li_2O	0	0	0.058645
MgO	0	0.010179	0.049686
MnO	0	0	0.020429
Na_2O	0.024833	0.202943	0.262441
P_2O_5	0	0.001206	0.04033
SiO_2	0.249328	0.419786	0.594038
SnO_2	0	0	0.050414
TiO_2	0	0	0.050695
V_2O_5	0	0	0.050761
ZnO	0	0.030387	0.053859
ZrO_2	0	0.035576	0.09312
Others	0	0.000203	0.034467
ln[k, in]	-6.21461	-3.45777	-1.66601
N_{ALK}	0.138104	0.22628	0.274326
N_{SiAl}	0.457015	0.561544	0.723558

2.4.2 Model

Due to the combination of data from two methods, the form of models considered is:

$$\ln[k] = k_s S_{0/1} + \sum_{i=1}^{q} k_i x_i + Selected\left\{\sum_{i=1}^{q} k_{ii} x_i^2 + \sum_{i=1}^{q}\sum_{j\neq i}^{q-1} k_{ij} x_i x_j\right\},$$

where k_s is an offset for k_{stat} data, $S_{0/1}$ is a static method counter = 0 for k_{bubb} and = 1 for k_{stat}, k_i is the i^{th} component coefficient, k_{ii} is the i^{th} component quadratic term, and k_{ij} is the i^{th}-j^{th} components cross-product coefficient. The component concentrations are represented by normalized mass fractions of the i^{th} component (x_i) where: $x_i = g_i / (1 - g_{Cl} - g_{SO_3})$.

A first order model was fitted to the data to determine which components had significant effects on ln[k_{1208}]. Al_2O_3, B_2O_3, CaO, Cr_2O_3, Fe_2O_3, Li_2O, MgO, MnO, Na_2O, P_2O_5, SiO_2, SnO_2, TiO_2, V_2O_5, ZnO, and ZrO_2 were found to have significant effects. The first order model had an R^2 = 0.805. A PQM was developed using stepwise regression. The model has the same 16 first order

terms as the first order model plus four second order terms: $Fe_2O_3 \times Fe_2O_3$, $Cr_2O_3 \times Na_2O$, $MgO \times SiO_2$, $Na_2O \times TiO_2$. This model was found to have the best fit statistics without overfitting with an $R^2 = 0.850$. The next most significant second order term ($B_2O_3 \times V_2O_5$) increases the R^2 to 0.856, respectively. The model coefficients are reported in Table 2-9. The predicted values are compared to measured values in Figure 2-11 and component effects are shown in Figure 2-12.

Table 2-9. Coefficients and summary statistics for ln[*k*, in] model with composition in normalized mass fractions.

Term	Coefficient	Statistic	Value
$S_{0/1}$	0.510251	n	358
Al_2O_3	-18.8275	p	22
B_2O_3	-2.23895	Mean ln[k_{1208}]	-3.57234
CaO	8.779949	R^2_{fit}	0.8503
Cr_2O_3	-296.638	R^2_{Adj}	0.8410
Fe_2O_3	10.96977	R^2_{press}	0.8248
Li_2O	52.95097	$RMSE_{fit}$	0.3063
MgO	-147.13	$RMSE_{press}$	0.3215
MnO	-25.5567	Pooled SD ln[k_{1208}]	0.3311
Na_2O	22.16205		
P_2O_5	-19.6081		
SiO_2	-14.8231		
SnO_2	-2.05913		
TiO_2	-39.9969		
V_2O_5	-9.56704		
ZnO	-12.3489		
ZrO_2	-9.90048		
Others	13.76996		
$Fe_2O_3 \cdot Fe_2O_3$	-114.49		
$Cr_2O_3 \cdot Na_2O$	1093.039		
$MgO \cdot SiO_2$	337.1618		
$Na_2O \cdot TiO_2$	190.5963		

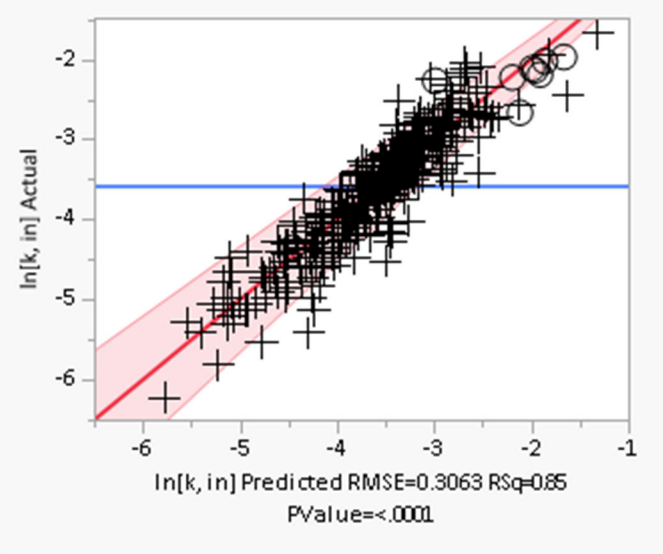

Figure 2-11. Predicted versus measured ln[k_{1208}, in]. Circles represent the APPS glass data.

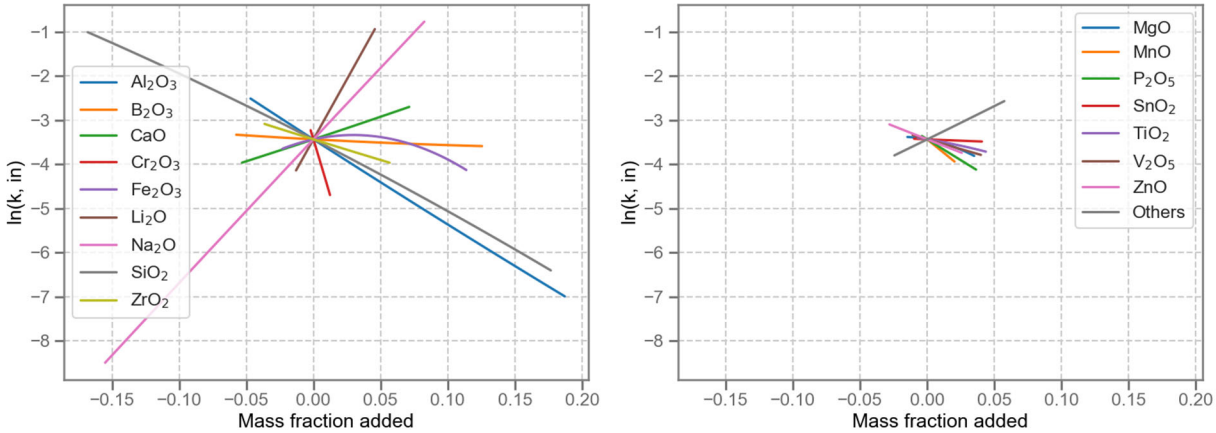

Figure 2-12. Component effects on ln[k_{1208}, in] (For Information Only).

2.5 P_2O_5 Constraint

High concentrations of phosphorous tend to cause immiscible liquid or crystalline phase separation in alkali-silicate waste glass melts (for examples see Bunnell 1988; Jantzen et al. 2000; Kot et al. 2007; Li et al. 1995, 1997a,b and 1998; and Langowski 1996). As the impacts of this phase separation on Hanford HLW glasses and melts are not fully understood, a constraint is needed to avoid their formation. The Hanford baseline HLW formulation algorithm employs three related constraints: $g_{P_2O_5} \le 0.045$, $g_{CaO} \times g_{P_2O_5} \le 0.00065$, and $g_{Li_2O} \le 0.06$ (Vienna and Kim 2014). The phosphate limit employed at the Defense Waste Processing Facility (DWPF) is $g_{P_2O_5} \le 0.0225$ (Edwards 2006) and the one at the West Valley Demonstration Project (WVDP) was $g_{P_2O_5} \le 0.0138$ (Barnes 2002). More recent data has suggested that all these constraints are likely to be overly conservative with glasses containing significantly higher P_2O_5 satisfying all constraints.

2.5.1 High P_2O_5 Model Data

Glasses with P_2O_5 ≥ 1 wt% and containing crystallization data were compiled from the reports described in Table 2-10. A total of 240 glasses were compiled. The distributions of component concentrations were evaluated using histograms for individual (1D) coverage and a scatterplot matrix for pair-wise (2D) coverage. It was determined that Al_2O_3, B_2O_3, Bi_2O_3, CaO, Cr_2O_3, Fe_2O_3, K_2O, Li_2O, MgO, MnO, Na_2O, NiO, P_2O_5, SiO_2, ZnO, and ZrO_2 had sufficient coverage to justify inclusion in modeling as independent terms. None of the rare earth oxides had sufficient coverage individually, however combined rare earth oxides $\left(g_{RE_2O_3} = g_{Ce_2O_3} + g_{Gd_2O_3} + g_{La_2O_3} + g_{Nd_2O_3}\right)$ did have sufficient coverage and therefore was included as an independent term. The range of each component concentration along with median value for the 240-glass dataset is given in Table 2-11.

Table 2-10. Summary of high (> 1 wt%) P_2O_5 HLW glass data

Study	# with P_2O_5 ≥ 1 wt%	Document
HLW-E-Bi	17	Matlack et al. 2007
HLW-E-Cr	20	Matlack et al. 2007
HLW-BP	10	Kot et al. 2007
HWI-AL	17	Matlack et al. 2008
HLW-E-ES	15	Matlack et al. 2009
HLW-E-M	13	Matlack et al. 2009
HLW-E-SP	3	Matlack et al. 2009
HWI-AL	9	Matlack et al. 2010
HLW-Bi	14	Matlack et al. 2010b
HLW-NG	9	Matlack et al. 2011
HWBi	24	Gan et al. 2012
HLW-CP	24	Gan et al. 2015
HLW-HP	17	Matlack et al. 2017
HLW-HPA	21	Matlack et al. 2017b

Study	# with P_2O_5 ≥ 1 wt%	Document
PNNL HLW-E	42	Rodriguez et al. 2011
APPS	6	Gervasio et al. 2024

Table 2-11. Range of high phosphate glass data used in model development, mass fraction

Oxide	Min	Median	Max
Al_2O_3	0.00989	0.12755	0.29509
B_2O_3	0.03956	0.14151	0.21930
Bi_2O_3	0.00000	0.02868	0.08717
CaO	0.00396	0.01073	0.20195
Cr_2O_3	0.00098	0.00579	0.06000
Fe_2O_3	0.00000	0.05687	0.11290
K_2O	0.00051	0.00663	0.15250
Li_2O	0.00000	0.02786	0.07951
MgO	0.00000	0.00137	0.05117
MnO	0.00000	0.00000	0.03530
Na_2O	0.00000	0.10523	0.23909
NiO	0.00000	0.00476	0.02967
P_2O_5	**0.01021**	**0.02759**	**0.08970**
SiO_2	0.17439	0.35334	0.46685
ZnO	0.00000	0.00108	0.04500
ZrO_2	0.00034	0.00168	0.07566
RE_2O_3	0.00000	0.00000	0.01112
Others	0.00663	0.01673	0.10497

2.5.2 Model

The data was individually evaluated to identify glasses that exceeded a phosphate solubility limit by either:

1) precipitating ≥ 1 vol% of a phosphate containing phase after an isothermal hold at 950°C or

2) forming ≥ 5 mass% phosphate-containing phase after canister centerline cooling (CCC), producing a ≥ 1 increase in the natural logarithm of PCT responses between quenched and CCC and did not form nepheline or eucryptite during CCC.

Of the 240 original glasses, 68 failed at least one of the phosphate related constraints (marked as Y) and 172 did not (marked as N). Most of the 68 failed glasses formed ≥ 1 vol% crystal at 950 °C. Of those, 52 glasses formed ≥ 2 vol% crystal at 950 °C.

Several modeling approaches were considered to separate the Y's from the N's based on glass composition including k-nearest neighbor, decision tree, random forest, support vector machine, and logistic regression. Of these approaches, logistic regression resulted in the most suitable

confusion matrix and had the added advantages of ease of implementation in a spreadsheet calculation and smooth composition-response functions which is ideal for optimizations.

The final model was a logistic regression with a logit link function and a PQM composition term:

$$\ln\left[\frac{P}{1-P}\right] = \sum_{i=1}^{n} p_i g_i + Selected\left\{\sum_{i=1}^{n} p_{ii} g_i^2 + \sum_{i=1}^{n}\sum_{j\neq i}^{n-1} p_{ij} g_i g_j\right\},$$

where: P is the probability of failing a phosphate related constraint and p_i, p_{ii}, and p_{ij} are the coefficients for component i, component i-squared, and component i-j cross-product; respectively.

The coefficients for the selected logistic regression are listed in Table 2-12 and component effects are shown in Figure 2-13. As anticipated, increasing concentration of CaO, P_2O_5, or RE_2O_3 increase P, while increasing concentration of Li_2O, Na_2O, or SiO_2 decrease P. Figure 2-14 shows the classification threshold plot and confusion matrix for this model. A threshold value of $P \leq 0.24$ (logit = $\ln[P/(1-P)] \leq -1.1527$) was selected because it results in less than 10% false negatives while minimizing false positives. Conveniently, this threshold also results in no false negatives from the APPS glasses (diamond points in the figure), although there are three false positives among the APPS glasses.

Table 2-12. Logistic regression model coefficient for phosphorous constraint

Term	Coefficient (p_i, p_{ij})
CaO	52.97384
Li_2O	-89.1373
Na_2O	149.5926
P_2O_5	45.90846
SiO_2	35.94944
RE_2O_3	140.3734
Others	-21.222
SiO_2·× Na_2O	-557.648
P-Threshold	0.24

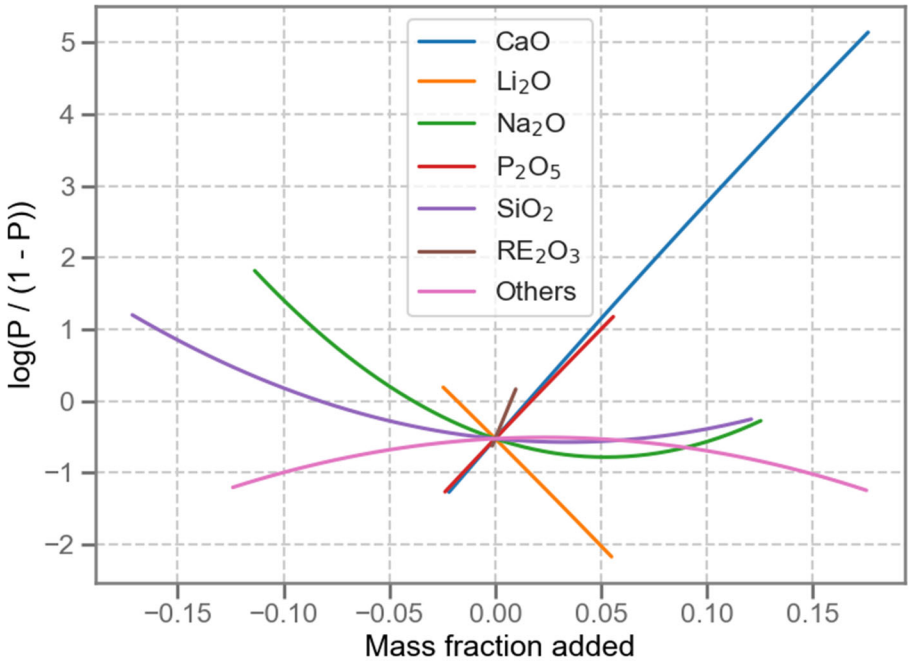

Figure 2-13. Component effects on phosphorous constraint logistic regression (For Information Only).

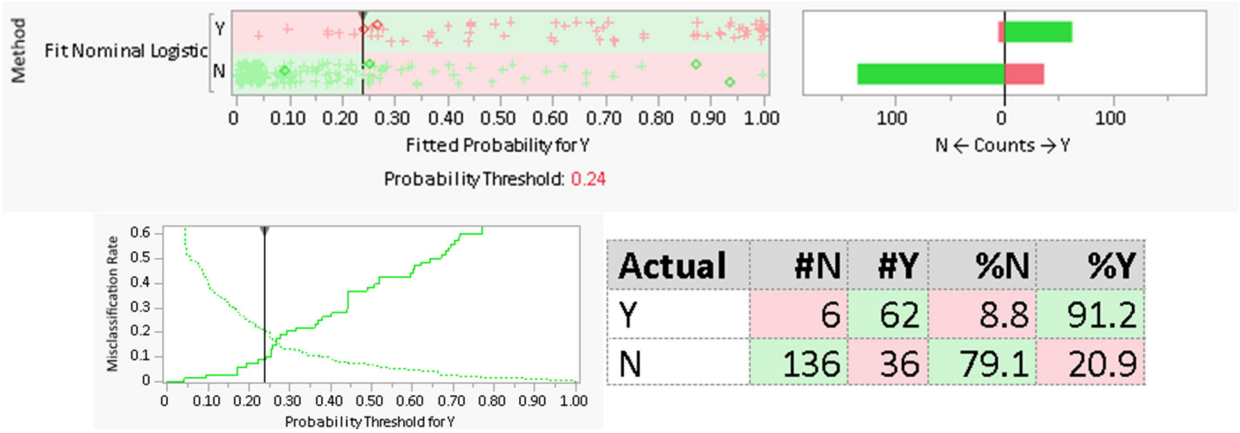

Actual	#N	#Y	%N	%Y
Y	6	62	8.8	91.2
N	136	36	79.1	20.9

Figure 2-14. Classification threshold plot and confusion matrix for phosphorous constraint red points fail the constraints, green points do not. Diamonds represent the 6 APPS glasses.

3.0 Formulation Methods and Constraints

This section summarizes the property constraints (Section 3.1), model validity ranges (Section 3.2) and optimization criteria (Section 3.3) for the EWG2.5 formulation algorithm. Example calculations can be found in Section 3.4. Constraints for EWG1 and EWG2 formulation algorithms can be found in Appendix A and Appendix B, respectively.

3.1 Property Constraints

A combination of models from the literature and those developed in this report are recommended to predict the properties of example DFHLW glasses while glass property data gaps are being filled. These models are summarized in Table 3-1.

Table 3-1. List of property constraints for DFHLW glass composition estimation

Property	Reference	Constraint	U_{pred} [8]	Note
PCT	Vienna and Crum (2018) This report, Section 2.1	$NL_{Ave} \leq 4$ g/m^2 $NL_{Ave} \leq 6.4368$ g/m^2	None 95% SUCI	[1]
TCLP	Kim and Vienna (2003)	$C_{Cd} \leq 0.48$ mg/L	None	[2]
Nepheline	Lu et al. (2021)	$p \geq 0.028$	None	[3]
Spinel	Vienna et al. (2016)	$T_{2\%} \leq 950$ °C	None	[4]
Zirconia	Vienna et al. (2016)	T_L-Zr ≤ 1050 °C (for $g_{ZrO2} \geq 0.04$)	None	[9]
Viscosity	This report, Section 2.2	$4 \leq \eta_{1150} \leq 6$ Pa·s $\eta_{1100} < 15$ Pa·s	90% CI 90% CI	
EC	This report, Section 2.2	$\varepsilon_{1100} \geq 0.1$ S/cm $\varepsilon_{1200} \leq 0.7$ S/cm	90% CI 90% CI	
Sulfate	This report, Section 2.3	$g_{SO3} \leq w_{SO3}$ - offset, wt%	95% CI	[5]
Immiscibility	Peeler and Hrma (1994)	$N_{NaLi} \geq 20$ wt%	None	[6]
K-3 Corrosion	This report, Section 2.4	$k_{1208} \leq 0.04$ in	95% CI	[7]
Phosphate	This report, Section 2.5	$p \leq 0.24$	95% CI	

Notes:

[1] The Ave ln[*NL*] of the DWPF EA glass is = (ln[8.350] + ln[6.675] + ln[4.785])/3 = 1.862. Applying an exponential function to Ave ln[*NL*] yields a $NL_{Ave} = 6.4368$ g/m^2 which will be used to limit PCT response for the model in this report. The model from Vienna and Crum (2018) will be added to cover primarily the composition region of higher Al_2O_3 concentrations. An artificial margin of 2.4368 g/m^2 is added to this model to compensate for U_{pred} for which the necessary data isn't supplied in the paper. The value of 4 g/m^2 is consistent with the original EWG formulation method (Vienna et al. 2016).

[2] The TCLP model was found to be conservative for APPS glasses, so no U_{pred} is applied.

[3] Lu et al. (2021) limits the probability of nepheline formation based on the compositional distance above a dividing line (p) the standard model with a limit of $p > 0$ results in a roughly 10% failure rate. Increasing the threshold to $p \geq 0.028$ reduces the failure rate to 0 for the model dataset and would exclude the two APPS glasses that precipitated nepheline.

[4] The original EWG limited the spinel fraction in glass to 2 vol% at 950 °C ($T_{2\%} \leq 950$ °C) which is less restrictive than the WTP baseline constraint of 1 vol% at 950 °C but adds considerable margin compared to the ≤ 4.5 vol% that could be acceptable (Matyas et al. 2013), the 4.2 vol% demonstrated in short term melter tests (Matlack et al. 2009) and the glass with 2 to 4 vol% demonstrated in long-term tests (Matyas et al. 2018).[1]

[5] The w_{SO3} model in this report was based on 3TS solubility data which have been shown to be 0.33 wt% SO_3 higher than the melter tolerance data as reported by Skidmore et al. (2019). Therefore, the predicted $g_{SO3} \leq w_{SO3} - 0.33$ is the bounding limit. Here, g_{SO3} is before accounting for any volatile loss of SO_3.

[6] Immiscibility limit is given by $N_{NaLi} = (g_{Na_2O} + 2.07 g_{Li_2O}) / (g_{Na_2O} + 2.07 g_{Li_2O} + g_{B_2O_3} + g_{SiO_2}) \geq$ 0.2 mass fraction.

[7] K-3 corrosion data was compiled from both static (k_{stat}) and bubbled (k_{bubb}) test methods. Most of the data is k_{bubb} as is the currently applied limit of $k_{bubb} \leq 0.04$ inch. Therefore, the test method offset Stat0/1 of 0 should be applied to model predictions.

[8] Prediction uncertainties (U_{pred}) are applied to the limits associated with all models generated in this report. They are calculated based on confidence intervals (CIs) at 90% confidence for processing related properties: $U_{pred} = t_{1-\alpha,n-p}\sqrt{\mathbf{g}^{\mathrm{T}}[s^2(\mathbf{G}^{\mathrm{T}}\mathbf{G})^{-1}]\,\mathbf{g}}$. For PCT response, a simultaneous upper confidence interval (SUCI) at 95% confidence interval: $U_{pred} = \sqrt{pF_{1-2\alpha,(p,n-p)}}\sqrt{\mathbf{g}^{\mathrm{T}}s^2(\mathbf{G}^{\mathrm{T}}\mathbf{G})^{-1}\mathbf{g}}$. The variance covariance matrices ($s^2[\mathbf{G}^{\mathrm{T}}\mathbf{G}]^{-1}$) are reported in Appendix C. PCT, sulfate, K-3 corrosion and phosphate and 1-sided intervals while viscosity and conductivity are 2-sided.

[9] A sigmoid function was added to the T_L-Zs model predictions to avoid a singularity in the first derivative of composition versus predicted response with 0 for $g_{ZrO2} < 0.04$ and much greater than zero predicted T_L-Zs for $g_{ZrO2} \geq 0.04$. The equation used is: $T_L - Zs = \frac{\sum T_i g_i}{1 + e^{-1000(g_{ZrO_2} - 0.039)}}$.

3.2 Model Validity Constraints

The empirical models used to predict DFHLW glass properties are only valid within the range of data used to develop and validate the models. These model validity (MV) ranges are summarized in Table 3-2. The "overall" limits in the last two columns are recommended to be used in EWG2.5. These limits were generally developed by taking the maximum of the minimum values for each property and likewise the maximum limit is the minimum of the maximums for individual properties. Some exceptions were made when multiple models were used for a given property and/or if the model was validated across a broader range. Some recommended models use compositions in mole fractions which are not given in the table. The range of validity does not directly translate into mole fractions; however, the key components were spot checked and found to be well bounded by the overall limits. In addition to the single component limits, some of the models have additional multi-component limits. These include:

- K-3 Corrosion Model: $N_{Alk} = g_{Na_2O} + 2.07 g_{Li_2O} + 0.66 g_{K_2O}$ is between 0.1381 and 0.2743

[1] Note: The glass testing in Matyas et al. (2018) had 2 to 4 vol% in multiple crucible melts run at 850 °C.

- K-3 Corrosion Model: $N_{SiAl} = g_{SiO_2} + 1.6970 g_{Al_2O_3}$ is between 0.4570 and 0.7236
- PCT Model: 0.1285 ≤ N_{Alk} ≤ 0.3010

In these cases, the normalized concentration ratios are based on ratios of molecular weights. Based on these data limits, it is recommended that the following multi-component limits be added:

- 0.1381 ≤ N_{Alk} ≤ 0.2743
- 0.4570 ≤ N_{SiAl} ≤ 0.7236

Table 3-2. Model validity constraints in mass fractions

Model	SO_3		Phosphate		Viscosity		Elec. Cond.		K-3 Corrosion	
Bound	Min	Max	Min	Max	Min	Max	Min	Max	Min	Max
Al_2O_3	0.0305	0.2639	0.0099	0.2951	0.0300	0.2621	0.0300	0.2621	0.0305	0.2644
B_2O_3	0.0402	0.2228	0.0396	0.2193	0.0400	0.2201	0.0400	0.2201	0.0403	0.2233
Bi_2O_3	-	-	0	0.0872	-	-	-	-	-	-
CaO	0	0.1292	0.0040	0.2020	0	0.1278	0	0.1271	0	0.1245
CdO	-	-	-	-	-	-	-	-	-	-
Cr_2O_3	-	-	0.0010	0.0600	-	-	-	-	0	0.0145
F	0.0004	0.0453	-	-	-	-	-	-	0	0.0453
Fe_2O_3	-	-	0	0.1129	0	0.1198	0	0.1198	0	0.1369
K_2O	0	0.0584	0.0005	0.1525	0	0.0809	0	0.0809	0	0.0813
Li_2O	0	0.0512	0	0.0795	0	0.0633	0	0.0633	0	0.0586
MgO	-	-	0	0.0512	0	0.0502	0	0.0502	0	0.0497
MnO	-	-	0	0.0353	-	-	-	-	0	0.0204
Na_2O	0.0923	0.2704	0	0.2391	0.0247	0.2692	0.0247	0.2689	0.0248	0.2624
NiO	-	-	0	0.0297	-	-	-	-	-	-
P_2O_5	0.0007	0.0403	0.0102	0.0897	0	0.0403	0	0.0403	0	0.0403
RE_2O_3	-	-	0	0.0111	-	-	-	-	-	-
SiO_2	0.2488	0.5936	0.1744	0.4669	0.2724	0.5850	0.2457	0.5850	0.2493	0.5940
SO_3	-	-	-	-	-	-	-	-	-	-
SrO	-	-	-	-	-	-	-	-	-	-
ThO_2	-	-	-	-	-	-	-	-	-	-
TiO_2	0	0.0294	-	-	0	0.0400	0	0.0500	0	0.0507
UO_3	-	-	-	-	-	-	-	-	-	-
V_2O_5	0	0.0573	-	-	0	0.0567	0	0.0571	0	0.0508
ZnO	-	-	0	0.0450	0	0.0582	0	0.0582	0	0.0539
ZrO_2	0	0.0930	0.0003	0.0757	0	0.0924	0	0.0924	0	0.0931
Others	0	0.0377	0	0.0522	0	0.0377	0	0.0377	0	0.0345

Table 3-2. cont. Model validity constraints in mass fractions

	PCT		$T_{2\%}$		2016 HLW overall (Vienna et al. 2016		EWG LAW Database + APPS 2024		**Overall Recommended**	
	Min	Max	Min	Max	Min	Max	Min	Max	**Min**	**Max**
Al_2O_3	0.0300	0.2632	0.0190	0.3000	0	0.3000	0.0300	0.2620	**0.03**	**0.3000**
B_2O_3	0.0400	0.2217	0.0300	0.2200	0.0400	0.2200	0.0392	0.0220	**0.04**	**0.2200**
Bi_2O_3	-	-	0	0.0738	0	0.0700	0	0.0493	**0**	**0.0700**
CaO	0	0.1292	0	0.1400	0	0.1000	0	0.1289	**0**	**0.1270**
CdO	-	-	0	0.0200	0	0.0150	0	0.0010	**-**	**-**
Cr_2O_3	0.0001	0.0144	0	0.0450	0	0.0300	0	0.0143	**0**	**0.0145**
F	0.0004	0.0452	0	0.0200	0	0.0250	0	0.0450	**0**	**0.0450**
Fe_2O_3	0	0.0685	0	0.2128	0	0.2000	0	0.1320	**0**	**0.1198**
K_2O	0	0.0584	0	0.0820	0	0.0600	0	0.0831	**0**	**0.0584**
Li_2O	0	0.0512	0	0.0632	0	0.0600	0	0.0632	**0**	**0.0512**
MgO	0	0.0506	0	0.0600	0	0.0600	0	0.1000	**0**	**0.0502**
MnO	-	-	0	0.0800	0	0.0800	0	0.0245	**0**	**0.0204**
Na_2O	0.0923	0.2704	0.0358	0.2500	0.0410	0.2400	0.0246	0.2693	**0.041**	**0.2700**
NiO	-	-	0	0.0300	0	0.0300	0	0.0790	**0**	**0.0297**
P_2O_5	0.0007	0.0399	0	0.0548	0	0.0450	0	0.0474	**0**	**0.0400**
RE_2O_3	-	-	0	0.0120	-	-	0	0.0777	**0**	**0.0111**
SiO_2	0.2476	0.5847	0.2000	0.5300	0.2200	0.5300	0.2457	0.5846	**0.2493**	**0.5300**
SO_3	0.0004	0.0177	0	0.0080	-	-	0	0.045	**0**	**0.0280**
SrO	-	-	0	0.1000	0	0.1010	0	0.0788	**-**	**0.0788**
ThO_2	-	-	0	0.0597	0	0.0600	-	-	**-**	**-**
TiO_2	0	0.0294	0	0.0525	0	0.0500	0	0.0500	**0**	**0.0294**
V_2O_5	0	0.0573	-	-	-	-	0	0.0570	**0**	**0.0508**
UO_3	-	-	0	0.0650	0	0.0630	0	-	**0**	**0.0630**
ZnO	0	0.0575	0	0.0450	0	0.0400	0	0.0579	**0**	**0.0400**
ZrO_2	0	0.0927	0	0.0960	0	0.1350	0	0.0924	**0**	**0.0924**
Others	0	0.0377	-	-	-	-	0	0.0377	**0**	**0.0377**

3.3 Optimization Criteria

The glass compositions are optimized by varying the concentrations of glass forming chemicals (GFCs) and waste to maximize the waste loading while simultaneously satisfying the property and composition constraints. Appendix D lists the nominal compositions of the current list of GFCs. Unguided optimization often results in selection of GFCs that are not ideal. For example, Cr_2O_3 addition in cases of low K-3 corrosion glasses or V_2O_5 addition in cases of low SO_3. To avoid these concerns, a logic statement is used in the optimization stating that V_2O_5 is not added in cases the glass is not sulfate salt-limited and a Cr_2O_3 limit of 0.6 wt% will be imposed if Cr_2O_3 is selected as an additive.

These optimization criteria will result in a reasonable set of glasses for design, testing, and planning purposes in the near-term. As data collection and modeling efforts continue, glass formulation approaches and compositions will evolve without jeopardizing the validity of work performed.

3.4 Example Calculations

To demonstrate the glass formulation approach suggested, example calculations are described here. Three example waste compositions were selected from the feed vector supplied by Britton (2023), summarized in Table 3-3. These waste compositions can also be found in Gervasio et al. (2024). Glass was optimized for each of these three example wastes. The formulations are summarized in Table 3-4, the resulting glass compositions in Table 3-5, and the predicted properties in Table 3-6.

Table 3-3. Composition of wastes used in example calculations.

Element concentrations mg/L waste				Simplified oxide composition mass fraction			
Batch	3	17	45	Batch	3	17	45
Ag	43.3828	0.0890	116.0695	Ag_2O	0.00017	2.76E-07	0.000472
Al	73273.1946	19554.1811	11217.8430	Al_2O_3	0.506138	0.106807	0.080257
As	20.9502	0	4.2409	B_2O_3	0.000623	0	0.002414
B	52.9313	0	198.0322	BaO	0.00012	7.67E-05	0.000265
Ba	29.3283	23.7491	62.7478	Bi_2O_3	0.001788	3.03E-05	0.000348
Be	1.0543	0	9.7194	CaO	0.007861	0.013103	0.003004
Bi	438.7217	9.4088	82.3612	CdO	2E-05	3.51E-10	1.2E-05
Ca	1536.7589	3239.3624	566.9987	Cl	0.003726	0.00453	0.007745
Cd	4.7966	0.0001	2.7725	Cr_2O_3	0.002525	0.002402	0.000966
Ce	51.0311	0	39.2768	F	0.004061	0.104781	0.071917
Cl	1019.3115	1567.1484	2045.3118	Fe_2O_3	0.066038	0.013945	0.060013
Co	18.6155	0	1.7833	K_2O	0.003881	0.006364	0.010779
Cr	472.5809	568.5712	174.5412	Li_2O	5.65E-05	0	1.01E-05
Cs	1.6185	3.4092	0.7476	MgO	0.000267	0	0.001611
Cu	24.8253	0	29.4530	MnO	0.006666	0.000311	0.005099
F	1110.8926	36246.3272	18993.2214	Na_2O	0.29061	0.6154	0.569473
Fe	12634.3842	3374.0543	11085.4985	LN_2O_3	0.001045	0.000296	0.001355
Hg	27.2056	0.4128	22.2984	NiO	0.006564	0.000595	0.002265
K	881.2057	1827.6148	2363.2796	P_2O_5	0.007112	0.023669	0.005366
La	86.6454	87.3509	133.0884	PbO	0.003531	0.000254	0.00252
Li	7.1744	0	1.2332	PdO	1.33E-05	0	1.71E-05
Mg	43.9815	0	256.5713	Rh_2O_3	4.74E-06	0	6.11E-06
Mn	1412.0844	83.2359	1042.8406	RuO_2	0.000138	6.76E-20	0.000178
Mo	14.4276	0	3.2274	SiO_2	0.059441	0.003471	0.008385
Na	58971.9253	157927.6577	111572.5979	SnO_2	0	0	0
Nd	82.4399	0	98.2523	SO_3	0.00517	0.09653	0.009433
Ni	1410.9099	161.8696	470.0576	SrO	0.000189	6.57E-05	0.00022
P	849.0461	3573.3234	618.4202	ThO_2	0.008035	4.69E-05	7.82E-05
Pb	896.7472	81.6873	617.8672	TiO_2	4.32E-05	0	4.82E-05
Ru	28.6912	0	35.6860	UO_3	0.008836	0.003284	0.013115
S	566.3686	13373.6800	997.7314	V_2O_5	6.67E-05	0	3.72E-05
Sb	12.9219	0	1.3889	ZnO	0.000135	0	0.000113
Se	21.5580	0.0132	2.8597	ZrO_2	0.004402	0.004024	0.142022
Si	7600.1715	561.2926	1035.1721	Others	0.000724	1.18E-05	0.000456
Sr	43.6239	19.2053	49.1663				
Ta	0.7407	0	0.9213				
Th	1931.5257	14.2681	18.1595				
Ti	7.0841	0	7.6249				
Tl	0.5901	0	1.2120				
U	2011.4186	945.3905	2882.3729				
V	10.2154	0	5.5095				

Element concentrations mg/L waste				Simplified oxide composition mass fraction
Y	7.4682	0.0009	13.9809	
Zn	29.5708	0	23.9755	
Zr	891.3368	1030.6157	27767.5773	
NO_2	21986.9784	35560.5701	40128.2311	
NO_3	40317.1760	63167.9058	76945.5745	
TOC	1546.0506	8021.5413	486.6238	

Table 3-4. Formulation of example glasses (fraction of component oxide in glass)

Component	Batch 3	Batch 17	Batch 45
Kyanite	0	0.009249	0.101709
Boric acid	0.219716	0.066234	0.105393
Wollastonite	0	0.213945	0
Na_2CO_3	0	0.047149	0
Li_2CO_3	0.013759	0.003212	0
Cr_2O_3	0	0.001655	0.005614
Silica	0.240252	0.386448	0.34796
Zincite	0.039941	0	0.039265
Zircon	0	0	0
V_2O_5	0	0.050809	0
Waste	0.486333	0.221299	0.400059

Table 3-5. Target glass composition in mass fraction of oxides and halogen, limiting values are bolded

Oxide	Batch 3	Batch 17	Batch 45
Ag_2O	0.00008	0	0.000189
Al_2O_3	0.24655	**0.0300**	0.090876
B_2O_3	**0.22**	0.066228	0.10635
BaO	0.00006	0.00002	0.000106
Bi_2O_3	0.00087	0	0.000139
CaO	0.003971	0.105503	0.001264
CdO	0.00001	0	0
Cl	0.001815	0.001017	0.003098
Cr_2O_3	0.001231	0.002193	**0.006**
F	0.001975	0.023188	0.028771
Fe_2O_3	0.03217	0.004109	0.024857
K_2O	0.001896	0.001424	0.004336
Li_2O	0.013619	0.003173	0
MgO	0.000153	0.000215	0.000687
MnO	0.003242	0.000285	0.00204
Na_2O	0.141397	0.18341	0.228237
LN_2O_3	0.000508	0.00007	0.000542
NiO	0.003192	0.000132	0.000906
P_2O_5	0.003459	0.005238	0.002147
PbO	0.001718	0.00006	0.001009

Oxide	Batch 3	Batch 17	Batch 45
PdO	0	0	0
Rh_2O_3	0	0	0
RuO_2	0.00007	0	0.00007
SiO_2	0.268581	0.499733	0.391917
SnO_2	0	0	0
SO_3	0.002543	0.021378	0.003783
SrO	0.00009	0.00001	0.00009
ThO_2	0.003908	0.00001	0.00003
TiO_2	0.00006	0.000183	0.000966
UO_3	0.004297	0.000727	0.005247
V_2O_5	0.00003	0.0508	0.00001
ZnO	**0.04**	0	0.039305
ZrO_2	0.002141	0.000891	0.056817

Table 3-6. Predicted glass properties, limiting values are bolded

Property	Model	Batch 3	Batch 17	Batch 45
$T_{2\%}$, °C	Vienna et al. (2016)	949	58.3	512
T_L-Zs, °C	Vienna et al. (2016)	0	0	781
PCT NL_{AVE}, g/m^2	Vienna & Crum (2018)	1.08	3.90	2.01
PCT NL_{Ave} (no *U*), g/m^2	This report	1.01	1.40	1.61
PCT NL_{Ave}+U_{pred}, g/m^2	This report	5.09	2.46	2.74
TCLP c_{Cd}, mg/L	Kim and Vienna (2003)	0.001	0	0.002
w_{SO3}-offset (no *U*), wt%	This report	0.459	2.27	0.560
w_{SO3}-offset (-U_{pred}), wt%	This report	0.2546	2.14	0.398
η_{1150} (no *U*), Pa.s	This report	5.71	4.13	5.82
η_{1150}+U_{pred}, Pa.s	This report	**6.00**	4.27	**6.00**
η_{1150}-U_{pred}, Pa.s	This report	5.44	**4.00**	5.65
η_{1100}+U_{pred}, Pa.s	This report	9.95	6.92	9.95
ε_{1150} (no U), S/cm	This report	0.28	0.38	0.60
ε_{1100}-U_{pred}, S/cm	This report	0.22	0.31	0.50
ε_{1200}+U_{pred}, S/cm	This report	0.35	0.46	**0.70**
NP *p*	Lu et al. (2021)	0.028	0.085	0.028
K-3 (no U), in	This report	0.004	0.032	0.035
K-3 +U_{pred}, in	This report	0.005	**0.04**	**0.04**
P_2O_5 *p*+U_{pred}	This report	0.13	**0.24**	0.001
Immisc N_{NaLi}, wt%	Peeler and Hrma (1994)	0.26	0.25	0.31

4.0 Conclusions

The EWG formulation method was developed in 2016 for application to pretreated wastes at the Hanford site (Vienna et al. 2016). It was applied to designing preliminary DFHLW glasses for the WTP and a subset of these glasses was tested to evaluate how well the models and constraints for pretreated wastes applied to DFHLW glasses (Gervasio et al. 2024). Measured property data for the 15 APPS glasses were only partially predicted by the original EWG models. The short comings were largely explained by the combination of LAW and HLW in the DFHLW feeds and therefore DFHLW glasses. A new set of models and constraints were developed for datasets that combined LAW glasses with DFHLW glasses. The following models were developed and validated:

- Product Consistency Test: Ave ln[NL] (Section 2.1)
- Viscosity: $\ln[\eta_T]$ (Section 2.2)
- Electrical Conductivity: $\ln[\varepsilon_T]$ (Section 2.2)
- Sulfur Solubility: $w_{SO3\text{-}3TS}$ (Section 2.3)
- K3-refractory neck corrosion: $\ln[k_{1208}]$ (Section 2.4)
- Phosphate solubility: logit[p] (Section 2.5)

These models were found to well predict the APPS glasses and when combined with literature models for HLW glass PCT (Vienna and Crum 2018), TCLP (Kim and Vienna 2003), nepheline (Lu et al. 2019), spinel formation (Vienna et al. 2016), zirconia containing phase liquidus temperature (Vienna et al. 2016), and immiscibility (Peeler et al. 1995) form the basis for near-term efforts to design and test DFHLW glasses. Optimization methods, constraints, and example calculations are described in Section 3.

It should be noted that although these models represent the current state-of-the-art for automated computational design of DFHLW glasses, they are not to be considered the final models for design of production glasses. There are several critical data gaps (Lu et al. 2023) that need to be experimentally filled including qualification of unqualified data and generation of new data to fill composition gaps. Once these gaps are filled, new models and constraints will be developed and validated for use in glass design and qualification for plant operation. It is anticipated that the new models will have both broader composition regions of validity and lower uncertainty.

5.0 References

10 CFR 830, *Nuclear Safety Management*. Code of Federal Regulations, as amended.

ASTM C1285, *Standard Test Methods for Determining Chemical Durability of Nuclear, Hazardous, and Mixed Waste Glasses and Multiphase Glass Ceramics: The Product Consistency Test (PCT).* ASTM International, West Conshohocken, PA.

ASTM C1720, *Standard Test Method for Determining Liquidus Temperature of Immobilized Waste Glasses and Simulated Waste Glasses*. ASTM International, West Conshohocken, PA.

Barnes SM. 2002. *WVDP Waste Form Qualification Report*, WVDP-186, Vol. 1.3, Rev. 3, West Valley Nuclear Services, West Valley, NY.

Bernards JK, GA Hersi, KT Pak, AJ Schubick, LM Bergmann, AN Praga, and SN Tilanus. 2021. *High-Level Waste Analysis of Alternatives Model Results Report*. RPP-RPT-61957, Rev. 2, Washington River Protection Solutions, Richland, WA.

Bernards JK, GA Hersi, TM Hohl, RT Jasper, PD Mahoney, NK Pak, SD Reaksecker, AJ Schubick, EB West, LM Bergmann, et al. 2020. *River Protection Project System Plan*. ORP-11242, Rev. 9, U.S. Department of Energy, Office of River Protection, Richland, WA.

Britton MD. 2023. *Revised DFHLW Washing and Blending Study Campaign Inventory*. WRPS-2300881, Washington River Protection Solutions, Richland, WA.

Bunnell, LR. 1988. *Laboratory Work in Support of West Valley Glass Development*, PNL-6539, Pacific Northwest Laboratory, Richland, WA.

Chow R. 1998. *Treatment of Underlying Hazardous Constituents in Toxicity Characteristic Metal (D004-D011) Wastes*, Memo to Record, dtd. 01/05/1998, U.S. Environmental Protection Agency, Washington, D.C.

Cook JR and DB Blumenkranz. 2003. *Data Quality Objectives Process in Support of LDR/Delisting at the WTP*. 24590-WTP-RPT-ENV-01-012, Rev. 1, River Protection Project, Hanford Tank Waste Treatment and Immobilization Plant, Richland, WA.

DOE. 1996. *Waste Acceptance Product Specifications for Vitrified High-Level Waste Forms (WAPS)*. DOE/EM-0093, U.S. Department of Energy, Office of Environmental Management, Washington, D.C.

DOE. 2000. *Design, Construction, and Commissioning of the Hanford Tank Waste Treatment and Immobilization Plant*. Contract DE-AC27-01RV14136, as amended, U.S. Department of Energy, Office of River Protection, Richland, WA.

DOE. 2013. *Hanford Tank Waste Retrieval, Treatment, and Disposition Framework*. U.S. Department of Energy, Washington, D.C.

DOE Order 414.1D, *Quality Assurance*. U.S. Department of Energy, Washington, D.C.

Dunst KP. 2020. *Process Inputs Basis of Design (PIBOD) for HLW*. 24590-HLW-DB-PET-19-001, Rev. 1, River Protection Project, Waste Treatment Plant, Richland, WA.

Edwards TB, KG Brown and RL Postles. 2006. *SME Acceptability Determination for DWPF Process Control (U)*. WSRC-TR-95-00364, Rev. 5, Savannah River National Laboratory, Aiken, SC.

EPA Method 1311, "Toxicity Characteristic Leaching Procedure (TCLP)." In *Test Methods for Evaluating Solid Waste, Physical/Chemical Methods*, EPA Publication SW–846.

Gan H, WK Kot and IL Pegg. 2012. *Development of High Waste-Loading HLW Glasses for High Bismuth Phosphate Wastes.* VSL-12R2550-1, The Catholic University of America, Washington, D.C.

Gan H, K Gilbo, AE Papathanassiu, WK Kot and IL Pegg. 2015. *Calcium Phosphate Constraints in HLW Glasses: Phosphate Liquidus Model.* VSL-15R3420-1, Vitreous State Laboratory at the Catholic University of America, Washington, D.C.

Gebhardt MJ. 2011. *APPS System Design Description*. 24590-WTP-SWD-PET-08-002, Rev. 5, River Protection Project, Waste Treatment Plant, Richland, WA.

Gervasio, V, JD Vienna, JB Lang, BE Westman, SE Sannoh, RL Russell, DS Kim, SC Cooley, J George, DA Cutforth, and SM Baird. 2021. *Enhanced Hanford Low-Activity Waste Glass Property Data Development: Phase 4*, PNNL-31556, Pacific Northwest National Laboratory, Richland, WA.

Gervasio, V, JD Vienna, JB Lang, DA Cutforth, NA Lumetta, X Lu, SK Cooley, SM Baird, and BE Westman. 2022. *Experimental Verification of the Preliminary Enhanced LAW Glass Formulation Algorithm*, PNNL-33233, Pacific Northwest National Laboratory, Richland, WA.

Gervasio, V, JJ Neeway, JD Vienna, JB Lang, BE Westman, JT Reiser, CE Lonergan, X Lu, SM Baird, DA Cutforth, and M Peterson. 2023. *Enhanced Hanford Low-Activity Waste Glass Property Data Development: Phase 5 and Phase 6*, PNNL-34331, Pacific Northwest National Laboratory, Richland, WA.

Gervasio, V, X Lu, JT Reiser, M Peterson, NL Canfield, JB Lang, JC Rigby, JL George, DA Cutforth, JM Westman, RA Brown, JM Oshiro, BK Boehnke, EA Cordova, JV Crum, NA Lumetta, and JD Vienna. 2024. *Direct Feed High-Level Waste APPS Model Glass Testing (DFHLW APPS) Matrix*, PNNL-35503, Pacific Northwest National Laboratory, Richland, WA.

Heredia-Langner A, V Gervasio, SK Cooley, CE Lonergan, DS Kim, AA Kruger, and JD Vienna. 2022. "Hanford low-activity waste glass composition-temperature-melt viscosity relationships." *International Journal of Applied Glass Science* 13(4):514-525.

Jantzen CM, NE Bibler, DC Beam, CL Crawford, and MA Pickett. 1993. *Characterization of the Defense Waste Processing Facility (DWPF) Environmental Assessment (EA) Glass Standard Reference Material (U)*. WSRC-TR-92-346, Rev. 1, Westinghouse Savannah River Company, Aiken, SC.

Jantzen, CM and KG Brown. 2000. "Predicting Phase Separation in Nuclear Waste Glasses," Ceramics Transactions, Vol. 107, 289-300 pp. American Ceramics Society.

Jin T, D Kim, LP Darnell, BL Weese, NL Canfield, M Bliss, MJ Schweiger, JD Vienna, and AA Kruger. 2019. “A crucible salt saturation method for determining sulfur solubility in glass melt.” *International Journal of Applied Glass Science* 10:92-102. https://doi.org/10.1111/ijag.12366

Kim DS and JD Vienna 2003. *Model for TCLP Releases from Waste Glasses*. PNNL-14061, Rev 1. Pacific Northwest National Laboratory, Richland, WA.

Kim DS and JD Vienna 2004. “Glass composition-TCLP response model for waste glasses”. In *Environmental Issues and Waste Management Technologies in the Ceramic & Nuclear Industries IX*: 297-305, American Ceramic Society.

Kim DS, JD Vienna, and AA Kruger. 2012. *Preliminary ILAW Formulation Algorithm Description*. 24590-LAW-RPT-RT-04-0003. Rev. 1, River Protection Project, Waste Treatment Plant, Richland, WA.

Kim DS, D Peeler, and P Hrma. 1995. “Effect of Crystallization on the Chemical Durability of Simulated Nuclear Waste Glasses.” In *Environmental Issues and Waste Management Technologies in the Ceramic and Nuclear Industries* 177-186.

Kot WK, L Myers and IL Pegg. 2007. *Baseline HLW Glass Formulations for Bismuth Phosphate Wastes*. VSL-07R1240-2, The Catholic University of America, Washington, D.C.

Kot WK, H Gan, M Chaudhuri and IL Pegg. 2011. *Glass Formulation for Next Generation Melters*. VSL-11R2310-1, Vitreous State Laboratory, the Catholic University of America, Washington, D.C.

Kot WK, K Gilbo, H Gan, and IL Pegg. 2019. *Enhancement of HLW Glass Property-Composition Models*. VSL-19R4480-1, Vitreous State Laboratory, The Catholic University of America, Washington, D.C.

Kroll JO, ZJ Nelson, CH Skidmore, DR Dixon, and JD Vienna. 2019. “Formulation of high-Al_2O_3 waste glasses from projected Hanford waste compositions.” *Journal of Non-Crystalline Solids* 517:17-25.

Langowski, MH. 1996. The Incorporation of P, S, Cr, F, Cl, I, Mn, Ti, U, and Bi into Simulated Nuclear Waste Glasses: Literature Study, PNNL-10980, Pacific Northwest National Laboratory, Richland, WA.

Li, H, MH Langowski, P Hrma, MJ Schweiger, JD Vienna, and DE Smith. 1995. *Minor Component Study for Simulated High-Level Nuclear Waste Glasses*, PNNL-10996, Pacific Northwest Laboratory, Richland, WA.

Li, H, JD Vienna, YL Chen, LQ Wang, and J Liu. 1997. "Phase Separation in Simulated Plutonium Glasses with Phosphate and Fluorine and the Effect on Glass Corrosion in Water," Scientific Basis for Nuclear Waste Management XX, Vol. 465, 277-283 pp. Materials Research Society, Pittsburgh, PA.

Li, H, YL Chen, and JD Vienna. 1997b. "Phase Separation in Borosilicate Glasses with P, F, S, and the Influence on Glass Durability in Aqueous Environments," Plutonium Futures – the Science, 113-114 pp. Los Alamos National Laboratory, Los Alamos, NM.

Li, H, JD Vienna, MJ Schweiger, and JV Crum. 1998. "Component Solubility in Lanthanide Borosilicate Glasses for the Vitrification of Plutonium Oxide and Plutonium-Bearing Materials," Ceramic Transactions, Vol. 87, 189-198 pp. American Ceramic Society, Westerville, OH.

Lonergan, CE, JL George, D Cutforth, T Jin, P Cholsaipant, SE Sannoh, CH Skidmore, BA Stanfill, SK Cooley, GF Piepel, RL Russell, and JD Vienna. 2019. *Enhanced Hanford Low-Activity Waste Glass Property Data Development: Phase 3*, PNNL-29847, Pacific Northwest National Laboratory, Richland, WA.

Lu X, I Sargin, and JD Vienna. 2021. “Predicting nepheline precipitation in waste glasses using ternary submixture model and machine learning.” *Journal of American Ceramic Society* 104:5636-5647.

Lu X and JD Vienna 2023. *Selection of Example DFHLW Glasses for Validation Tests*, Memo to RL Hanson, dtd 7/26/2023. CCN-335241. River Protection Project, Waste Treatment Plant, Richland, WA.

Lu, X, ZD Weller, V Gervasio, and JD Vienna. 2024. "Glass Design Using Machine Learning Property Models with Prediction Uncertainties: Nuclear Waste Glass Formulation," Journal of Non-Crystalline Solids, Accepted, DOI: 10.1016/j.jnoncrysol.2024.122907.

Matlack KS, H Gan, W Gong, IL Pegg, CC Chapman and I Joseph. 2007. *High Level Waste Vitrification System Improvements*: VSL-07R1010-1. ORP-56297, Vitreous State Laboratory, the Catholic University of America, Washington, D.C.

Matlack KS, H Gan, M Chaudhuri, WK Kot, W Gong, T Bardakci, IL Pegg and I Joseph. 2008. *Melt Rate Enhancement for High Aluminum HLW Glass Formulations*: VSL-08R1360-1. ORP-44236, Vitreous State Laboratory, the Catholic University of America, Washington, D.C.

Matlack KS, WK Kot, W Gong, W Lutze, IL Pegg and I Joseph. 2009. *Effects of High Spinel and Chromium Oxide Crystal Contents on Simulated HLW Vitrification in DM100 Melter Tests*: VSL-09R1520-1. ORP-56327, Vitreous State Laboratory, the Catholic University of America, Washington, D.C.

Matlack KS, H Gan, M Chaudhuri, WK Kot, W Gong, T Bardakci, IL Pegg and I Joseph. 2010. *DM100 and DM1200 Melter Testing with High Waste Loading Glass Formulations for Hanford High-Aluminum HLW Streams*: VSL-10R1690-1. ORP-44198, Vitreous State Laboratory, the Catholic University of America, Washington, D.C.

Matlack KS, H Gan, WK Kot, M Chaudhuri, RK Mohr, DA McKeown, T Bardakci, W Gong, AC Buechele, IL Pegg and I Joseph. 2010b. *Tests with High-Bismuth HLW Glasses*. VSL-10R1780-1, Vitreous State Laboratory, the Catholic University of America, Washington, D.C.

Matlack, KS, WK Kot, and IL Pegg. 2017. *High Waste Loading Glass Formulation Development for High-P HLW*, VSL-17R3700-1, The Catholic University of America, Washington, D.C.

Matlack, KS, WK Kot, and IL Pegg. 2017b. *Glass Formulation Development for Al, Fe, and Na Phosphate HLW*, VSL-17R4130-1, The Catholic University of America, Washington, D.C.

Matyas, J, DP Jansik, AT Owen, CA Rodriguez, JB Lang and AA Kruger 2013. Impact of Particle Agglomeration on Accumulation Rates in the Glass Discharge Riser of HLW Melter. In *Ceramics Transactions,* Vol. 241:59-68.

Matyas, J, GJ Sevigny, JJ Venarsky, JM Davis, CD Lukins, JB Lang, MK Edwards, CW Stewart, SE Sannoh, TG Veldman, NR Phillips and CM Fischer. 2018. *Evaluation of Crystal Accumulation in High-Level Waste Glasses with Research-Scale Melter*. PNNL-27419, Pacific Northwest National Laboratory, Richland, WA.

Mellinger GB and JL Daniel. 1984. *Approved Reference and Testing Materials for Use in Nuclear Waste Management Research and Development Programs*. PNL-4955-2, Pacific Northwest Laboratory, Richland, WA. https://doi.org/10.2172/6224421

Muller IS, K Gilbo, M Chaudhuri, and IL Pegg. 2018. *K-3 Refractory Corrosion and Sulfate Solubility Model Enhancement*. VSL-18R4360-1, Rev. 0, Vitreous State Laboratory, The Catholic University of America, Washington, D.C.

NQA-1-2012, *Quality Assurance Requirements for Nuclear Facility Application*. American Society of Mechanical Engineers, New York, NY.

Parsons. 2023. *Waste Treatment and Immobilization Plant High Level Waste Treatment Analysis of Alternatives*. DE-NA0002895, Parsons Corporation, Boston, MA.

Peeler DK and P Hrma 1994. “Predicting liquid immiscibility in multicomponent nuclear waste glasses.” *Ceramics Transactions* 45:219-229.

Perez JM. 2006. “Practical and Historical Bases for a Glass Viscosity Range for Joule-Heater Ceramic Melter Operation.” Email to JD Vienna, Pacific Northwest National Laboratory, Dec. 22, 2006. CCN: 150054, River Protection Project, Waste Treatment Plant, Richland, WA.

Petkus LL. 2003. “Canister Centerline Cooling Data, Revision 1.” To C.A. Musick, Oct. 29, 2003. CCN: 074851, River Protection Project, Waste Treatment Plant, Richland, WA.

Piepel GF, A Heredia-Langner, and SK Cooley. 2008. “Property–composition–temperature modeling of waste glass melt data subject to a randomization restriction.” *Journal of the American Ceramic Society* 91(10):3222-3228.

Rieck BT. 2018. *ILAW Product Qualification Report – Waste Forming Testing*. 24590-LAWRPT-PENG-17-008-05, Rev 1, River Protection Project, Waste Treatment Plant. Richland, WA.

Rodriguez CP, J McCloy, MJ Schweiger, JV Crum and A Winschell. 2011. *Optical basicity and nepheline crystallization in high alumina glasses*. PNNL-20184, Pacific Northwest National Laboratory, Richland, WA.

Russell, RL, T Jin, BP McCarthy, LP Darnell, DE Rinehart, CC Bonham, V Gervasio, JL Mayer, CL Arendt, JB Lang, MJ Schweiger, and JD Vienna. 2017. *Enhanced Hanford Low-Activity Waste Glass Property Data Development: Phase I*, PNNL-26630, Pacific Northwest National Laboratory, Richland, WA.

Russell, RL, BP McCarthy, SK Cooley, EA Cordova, SE Sannoh, V Gervasio, MJ Schweiger, JB Lang, CH Skidmore, CE Lonergan, BA Stanfill, and JD Vienna. 2021. *Enhanced Hanford*

Low-Activity Waste Glass Property Data Development: Phase 2, PNNL-28838, Rev. 2, Pacific Northwest National Laboratory, Richland, WA.

Russell, RL, JD Vienna, SM Baird, and DA Cutforth. 2022. *Hanford Low-Activity Waste Glass Minor Component Concentration Boundary Expansion*, PNNL-32826, Pacific Northwest National Laboratory, Richland, WA.

Skidmore CH, JD Vienna, T Jin, DS Kim, BA Stanfill, KM Fox, and AA Kruger. 2019. "Sulfur solubility in low activity waste glass and its correlation to melter tolerance." *International Journal of Applied Glass Science*, 10(4): 558-568.

Smith GL. 1993. *Characterization of Analytical Reference Glass-1 (ARG-1)*. PNL-8992, Pacific Northwest Laboratory, Richland, WA.

Vienna JD. 2008. "Phosphorous Limit in High-Level Waste Glass -- Supersedes CCN: 177731." CCN: 184901, River Protection Project, Waste Treatment Plant, Richland, WA.

Vienna JD and DS Kim. 2014. *Preliminary IHLW Formulation Algorithm Description*. 24590-HLW-RPT-RT-05-001, Rev. 1, River Protection Project, Waste Treatment Plant, Richland, WA.

Vienna JD and JV Crum. 2018. "Non-linear effects of alumina concentration on Product Consistency Test response of waste glasses." *Journal of Nuclear Materials* 511:396-405.

Vienna JD, A Fluegel, DS Kim, and P Hrma. 2009. *Glass Property Data and Models for Estimating High-Level Waste Glass Volume*. PNNL-18501, Pacific Northwest National Laboratory, Richland, WA.

Vienna JD, A Heredia-Langner, SK Cooley, AE Holmes, DS Kim, and NA Lumetta. 2022. *Glass Property-Composition Models for Support of Hanford WTP LAW Facility Operation*. PNNL-30932, Rev. 2, Pacific Northwest National Laboratory, Richland, WA.

Vienna JD, DS Kim, DC Skorski, and J Matyas. 2013. *Glass Property Models and Constraints for Estimating the Glass to be Produced at Hanford by Implementing Current Advanced Glass Formulation Efforts*. PNNL-22631, Rev. 1, ORP-58289, Pacific Northwest National Laboratory, Richland, WA.

Vienna JD, DS Kim, IS Muller, GF Piepel, and AA Kruger. 2014. "Toward understanding the effect of low-activity waste glass composition on sulfur solubility." *Journal of the American Ceramic Society* 97(10):3135–3142.

Vienna JD, GF Piepel, DS Kim, JV Crum, CE Lonergan, BA Stanfill, BJ Riley, SK Cooley, and T Jin. 2016. *Update of Hanford Glass Property Models and Constraints for Use in Estimating the Glass Mass to be Produced at Hanford by Implementing Current Enhanced Glass Formulation Efforts*. PNNL-25835, Pacific Northwest National Laboratory, Richland, WA.

Vienna JD, JO Kroll, P Hrma, JB Lang, and JV Crum. 2017. "Submixture model to predict nepheline precipitation in waste glasses." *International Journal of Applied Glass Science* 8(2):143-157.

Vienna JD, P Hrma, A Jiricka, DE Smith, TH Lorier, IA Reamer, and RL Schultz. 2001. *Hanford Immobilized LAW Product Acceptance Testing: Tanks Focus Area Results*. PNNL-13744, Pacific Northwest National Laboratory, Richland, WA.

Vienna JD, X Lu, P Ferkl, J Marcial, MS Fountain, M Trenidad, R Hanson, MD Britton, L Cree, and W Abdul. 2023. “High-Level Waste Glass Processing over Broad Range of Alternative Feed Compositions.” In *Proceedings of the 2023 Waste Management Symposia*, Phoenix, AZ.

Westesen AM, EL Campbell, SK Fiskum, AM Carney, TT Trang-Le, and RA Peterson. 2022. “Impact of feed variability on cesium removal with multiple actual waste samples from the Hanford site.” *Separation Science and Technology* 57(15). https://doi.org/10.1080/01496395.2022.2059378

Appendix A – EWG1 Formulation Constraints

Property and composition constraints were reported previously by Vienna et al (2016) and Vienna et al (2023).

Table A 1. Summary of property limits used in EWG1 formulation.

Constraint	Limit
Product consistency test (PCT) normalized element release (r_α)	$\ln[r_B\ (g/m^2)] \le 1.386$[(a)] $\ln[r_{Na}\ (g/m^2)] \le 1.386$[(a)] $\ln[r_{Li}\ (g/m^2)] \le 1.386$[(a)]
Probability of nepheline formation (p)	$p \le 0.3$ (probability)
Temperature at 2 vol% spinel ($T_{2\%}$)	$T_{2\%} \le 950$ °C
Liquidus temperature for zirconium-containing phases (T_L-Zr)	T_L-Zr ≤ 1050 °C if $g_{ZrO_2} > 0.04$
Viscosity at 1150 °C (η_{1150})	$1.386 \le \ln(\eta_{1150,}\ Pa{\cdot}s) \le 1.792$[(b)]
Combined P_2O_5 and CaO concentrations	$g_{P_2O_5} \times g_{CaO} \le 0.00065$ (mass fraction)^2
SO_3 concentration below solubility limit	$g_{SO_3} \le g_{SO_3}^{Limit}$
Cr_2O_3 concentration to avoid excessive Eskolaite formation	$g_{Cr_2O_3} \le 0.03$
Combined B_2O_3 and SiO_2 concentrations	$g_{SiO_2} + g_{B_2O_3} \ge 0.32$
Combined noble metal concentrations	$g_{PdO} + g_{Rh_2O_3} + g_{RuO_2} \le 0.0025$

(a) Corresponds to $r_\alpha \le 4$ g/m^2 (or 8 g/L in normalized loss units).
(b) Corresponds to $4 \le \eta_{1150} \le 6$ Pa·s.

Table A 2. Single component model validity constraints in mass fraction of oxide or halogen in glass.

Component	Min	Max
Al_2O_3	0.019	0.300
B_2O_3	0.040	0.220
Bi_2O_3	0	0.070
CaO	0	0.100
CdO	0	0.015
Cr_2O_3	0	0.030
F[(a)]	0	0.045
Fe_2O_3	0	0.200
K_2O	0	0.060
Li_2O	0	0.060
MgO	0	0.060
MnO	0	0.080
Na_2O	0.041	0.240
NiO	0	0.030
P_2O_5	0	0.045
SiO_2	0.220	0.530
SrO	0	0.101

Component	Min	Max
ThO_2	0	0.060
TiO_2	0	0.050
UO_3	0	0.063
V_2O_5[(b)]	0	0.04056
ZnO	0	0.040
ZrO_2	0	0.135

(a) F was increased from 2.5 to 4.5 wt%.
(b) Model validity limit from the HLW SO_3 solubility model in Vienna et al. (2016) for V_2O_5 (≤ 4.056 wt%).

Appendix B – EWG2 Formulation Constraints

Property and composition constraints were reported previously by Gervasio et al (2024).

In addition to the constraints and models described for the EWG1 process, the following sets of models were used:

- PCT response models: Vienna and Crum (2018), Kot et al. (2019), and Vienna et al. (2022)
- SO_3 solubility models: Vienna et al. (2022), Vienna et al. (2013)
- Viscosity models: Vienna et al. (2022), Kot et al. (2019)
- EC models (not included in Vienna et al. (2016)): Vienna et al. (2009), Vienna et al. (2022), Kot et al. (2019)
- Nepheline: Lu et al. (2021)
- Immiscibility: Peeler and Hrma (1994)
- K-3 corrosion (not included in Vienna et al. (2016)): Vienna et al. (2022)

With these additional models, the two most significant controlling variable constraints (Na_2O and $CaO \times P_2O_5$) were relaxed. Also, V_2O_5 was not used as a GFC unless the composition was SO_3 solubility limited. Li_2O, ZnO and MgO were only included as GFCs if they increased WL by ≥ 0.1 wt% absolute over the formulations without these additives. Combined, this formulation approach is referred to as second iteration of enhanced waste glass or EWG2.

Appendix C – Variance-Covariance Matrices

Table C 1. Variance Covariance Table for PCT Model

Term	Al_2O_3	B_2O_3	CaO	Li_2O	Na_2O	SiO_2	SnO_2	V_2O_5	ZnO	ZrO_2	Others	$Al_2O_3xAl_2O_3$	Al_2O_3xCaO
Al_2O_3	17.556857	-0.520165	4.847401	-0.900333	-1.120902	-0.890842	-0.371506	-1.332992	-1.291432	-1.279582	-0.677827	-71.487662	-79.089583
B_2O_3	-0.520165	1.171781	-0.469709	-0.030141	-0.008366	-0.128355	-0.155686	-0.334844	0.108266	-0.271741	-0.014482	-1.21848	7.876648
CaO	4.847401	-0.469709	4.477875	0.193223	-0.125316	-0.557567	0.367049	-1.174395	0.477271	-0.347218	-0.135453	-13.906403	-53.083363
Li_2O	-0.900333	-0.030141	0.193223	10.953705	2.288556	-0.853212	-2.2927	-1.24569	-0.848442	-0.400056	-1.084892	0.493906	-3.815503
Na_2O	-1.120902	-0.008366	-0.125316	2.288556	0.994745	-0.292606	-0.564449	-0.087234	-0.520276	-0.326546	-0.218035	3.55944	2.040836
SiO_2	-0.890842	-0.128355	-0.557567	-0.853212	-0.292606	0.302387	0.111295	0.044168	0.120929	0.092472	0.024931	3.907135	5.959442
SnO_2	-0.371506	-0.155686	0.367049	-2.2927	-0.564449	0.111295	4.820939	0.509622	-0.222217	-0.199128	0.023611	4.296407	-2.001896
V_2O_5	-1.332992	-0.334844	-1.174395	-1.24569	-0.087234	0.044168	0.509622	5.086576	-0.443899	0.584246	-0.176934	6.979949	14.052565
ZnO	-1.291432	0.108266	0.477271	-0.848442	-0.520276	0.120929	-0.222217	-0.443899	5.162028	0.1112	-0.020844	6.465928	-1.533929
ZrO_2	-1.279582	-0.271741	-0.347218	-0.400056	-0.326546	0.092472	-0.199128	0.584246	0.1112	3.037259	-0.038565	7.768696	2.387095
Others	-0.677827	-0.014482	-0.135453	-1.084892	-0.218035	0.024931	0.023611	-0.176934	-0.020844	-0.038565	1.335939	1.602863	5.158104
$Al_2O_3xAl_2O_3$	-71.487662	-1.21848	-13.906403	0.493906	3.55944	3.907135	4.296407	6.979949	6.465928	7.768696	1.602863	334.945844	243.044507
Al_2O_3xCaO	-79.089583	7.876648	-53.083363	-3.815503	2.040836	5.959442	-2.001896	14.052565	-1.533929	2.387095	5.158104	243.044507	803.438313

Table C 2. Variance Covariance Table for Viscosity Model

Terms	A	Al_2O_3	B_2O_3	CaO	Fe_2O_3	K_2O	Li_2O	MgO	Na_2O
A	0.003884	-9.73985	-2.31342	-2.48876	-4.66239	-3.58474	7.742809	-5.14091	-1.51916
Al_2O_3	-9.73985	26808.22	5244.881	6154.216	11976.08	8799.592	-21749.3	12621.38	2963.362
B_2O_3	-2.31342	5244.881	3543.986	1490.975	2845.469	2263.16	-4857.91	2817.21	866.3616
CaO	-2.48876	6154.216	1490.975	2877.09	3227.768	2440.022	-5666.71	3642.777	1022.911
Fe_2O_3	-4.66239	11976.08	2845.469	3227.768	8562.326	4188.148	-9134.46	5261.623	1897.829
K_2O	-3.58474	8799.592	2263.16	2440.022	4188.148	7441.328	-5679.22	4675.115	1758.19
Li_2O	7.742809	-21749.3	-4857.91	-5666.71	-9134.46	-5679.22	31859.8	-12257.1	798.479
MgO	-5.14091	12621.38	2817.21	3642.777	5261.623	4675.115	-12257.1	20283.57	2163.851
Na_2O	-1.51916	2963.362	866.3616	1022.911	1897.829	1758.19	798.479	2163.851	1891.443
P_2O_5	-6.5925	16931.89	3558.015	4219.834	7706.291	6248.469	-13073.4	8411.799	2452.886
SiO_2	-8.33364	21290.75	4615.916	5107.75	9760.611	7546.989	-18126.7	10912.37	2834.615
SnO_2	-6.82787	18075.37	4121.875	4837.186	9106.799	4310.46	-17279.9	7974.172	1594.257
TiO_2	-4.55263	11823.78	3156.494	4070.214	3446.902	2895.411	-9634.51	1901.351	1408.887
V_2O_5	-3.87383	10177.87	1848.077	2020.654	5841.599	3117.155	-9756.53	3530.076	654.1165
ZnO	-3.97059	10031.83	1850.392	2820.941	4482.175	3051.741	-10144.4	3586.835	1083.324
ZrO_2	-8.01786	19806.75	4827.525	5268.064	10388.75	7047.481	-16923.4	11349.42	2570.772
Others	-5.03553	12624.83	2733.55	3032.746	6253.538	4170.573	-12675.5	7646.545	819.3844
T_0	0.754455	-1922.92	-447.667	-481.804	-915.167	-698.312	1552.414	-1008.87	-287.928
Term	P_2O_5	SiO_2	SnO_2	TiO_2	V_2O_5	ZnO	ZrO_2	Others	T_0
A	-6.5925	-8.33364	-6.82787	-4.55263	-3.87383	-3.97059	-8.01786	-5.03553	0.754455
Al_2O_3	16931.89	21290.75	18075.37	11823.78	10177.87	10031.83	19806.75	12624.83	-1922.92
B_2O_3	3558.015	4615.916	4121.875	3156.494	1848.077	1850.392	4827.525	2733.55	-447.667
CaO	4219.834	5107.75	4837.186	4070.214	2020.654	2820.941	5268.064	3032.746	-481.804
Fe_2O_3	7706.291	9760.611	9106.799	3446.902	5841.599	4482.175	10388.75	6253.538	-915.167
K_2O	6248.469	7546.989	4310.46	2895.411	3117.155	3051.741	7047.481	4170.573	-698.312
Li_2O	-13073.4	-18126.7	-17279.9	-9634.51	-9756.53	-10144.4	-16923.4	-12675.5	1552.414
MgO	8411.799	10912.37	7974.172	1901.351	3530.076	3586.835	11349.42	7646.545	-1008.87
Na_2O	2452.886	2834.615	1594.257	1408.887	654.1165	1083.324	2570.772	819.3844	-287.928
P_2O_5	36328.14	14067.96	9652.771	7408.387	6307.826	8162.971	14468.96	4532.19	-1285.39
SiO_2	14067.96	18411.35	14870.5	9347.045	8432.327	8277.235	17175.32	10669.91	-1643.24
SnO_2	9652.771	14870.5	20585.29	9506.993	6655.436	8912.255	12761.86	10608.94	-1337.19
TiO_2	7408.387	9347.045	9506.993	26448.53	6524.754	5588.151	10861.66	5609.304	-889.198
V_2O_5	6307.826	8432.327	6655.436	6524.754	12783.37	4827.456	9517.834	3335.92	-749.497
ZnO	8162.971	8277.235	8912.255	5588.151	4827.456	13650.64	7274.079	7930.022	-780.647
ZrO_2	14468.96	17175.32	12761.86	10861.66	9517.834	7274.079	22744.28	10337.21	-1586.03
Others	4532.19	10669.91	10608.94	5609.304	3335.92	7930.022	10337.21	27376.61	-985.957
T_0	-1285.39	-1643.24	-1337.19	-889.198	-749.497	-780.647	-1586.03	-985.957	149.9128

Table C 3. Variance-Covariance Matrix for Electrical Conductivity Model

Term	A	Al_2O_3	B_2O_3	CaO	Fe_2O_3	K_2O	Li_2O	MgO	Na_2O
A	0.003452	-8.22653	-6.30082	-7.50509	-5.84019	-4.36891	9.935613	-5.12819	2.795787
Al_2O_3	-8.22653	21856.37	14578.74	18064.13	13989.48	10463.32	-26095.9	12329.33	-7649.06
B_2O_3	-6.30082	14578.74	13675.88	13996.43	10748.64	8026.816	-18871.1	9292.948	-5307.23
CaO	-7.50509	18064.13	13996.43	17940.49	13149.11	9892.441	-23235.8	11475.76	-6325.72
Fe_2O_3	-5.84019	13989.48	10748.64	13149.11	13204.76	7501.322	-16554.4	8042.451	-4590.36
K_2O	-4.36891	10463.32	8026.816	9892.441	7501.322	9831.653	-11758.2	6240.056	-3390.08
Li_2O	9.935613	-26095.9	-18871.1	-23235.8	-16554.4	-11758.2	46627.88	-17355.4	12423.69
MgO	-5.12819	12329.33	9292.948	11475.76	8042.451	6240.056	-17355.4	20351.17	-4467.78
Na_2O	2.795787	-7649.06	-5307.23	-6325.72	-4590.36	-3390.08	12423.69	-4467.78	3805.148
P_2O_5	-8.77878	21415.35	15837.43	19176.17	14742.93	11509.65	-25834.1	13175.83	-7561.53
SiO_2	-7.47402	18283.73	13471.61	16247.36	12428.43	9416.492	-23249.8	11073.84	-6683.54
SnO_2	-9.09247	22411.65	17146.09	20418.3	16372.08	9857.242	-29621.3	13021.17	-8502.91
TiO_2	-5.36358	13253.17	10279.82	12710.41	6564.541	5119.866	-17055.8	4841.514	-4843.73
V_2O_5	-4.33983	10834.07	7656.391	9081.155	8422.419	5165.678	-14492.8	5176.13	-4222.95
ZnO	-4.51344	10690.35	8062.601	10141.89	7233.355	5001.741	-15092.3	5694.398	-4070.26
ZrO_2	-7.44613	17432.99	13795.3	16643.24	13468.84	9267.485	-22494.8	11611.56	-6738.59
Others	-4.57429	10524.23	7888.761	9780.814	7951.075	5442.393	-15548.8	8806.837	-4856.79
T_0	-1.93904	4720.736	3598.358	4302.879	3332.066	2488.017	-5786.77	2925.091	-1658.6
Term	P_2O_5	SiO_2	SnO_2	TiO_2	V_2O_5	ZnO	ZrO_2	Others	T_0
A	-8.77878	-7.47402	-9.09247	-5.36358	-4.33983	-4.51344	-7.44613	-4.57429	-1.93904
Al_2O_3	21415.35	18283.73	22411.65	13253.17	10834.07	10690.35	17432.99	10524.23	4720.736
B_2O_3	15837.43	13471.61	17146.09	10279.82	7656.391	8062.601	13795.3	7888.761	3598.358
CaO	19176.17	16247.36	20418.3	12710.41	9081.155	10141.89	16643.24	9780.814	4302.879
Fe_2O_3	14742.93	12428.43	16372.08	6564.541	8422.419	7233.355	13468.84	7951.075	3332.066
K_2O	11509.65	9416.492	9857.242	5119.866	5165.678	5001.741	9267.485	5442.393	2488.017
Li_2O	-25834.1	-23249.8	-29621.3	-17055.8	-14492.8	-15092.3	-22494.8	-15548.8	-5786.77
MgO	13175.83	11073.84	13021.17	4841.514	5176.13	5694.398	11611.56	8806.837	2925.091
Na_2O	-7561.53	-6683.54	-8502.91	-4843.73	-4222.95	-4070.26	-6738.59	-4856.79	-1658.6
P_2O_5	51143.95	19233.52	20470.51	12704.25	10845.96	12569.97	20614.53	6075.249	5025.565
SiO_2	19233.52	16749.93	20061.73	11365.79	9569.723	9525.438	16093.3	9802.373	4281.325
SnO_2	20470.51	20061.73	32052.24	15328.98	11594.78	13643.69	18854.16	12974.22	5226.093
TiO_2	12704.25	11365.79	15328.98	29310.87	8085.133	7491.974	12673.07	7129.218	3029.404
V_2O_5	10845.96	9569.723	11594.78	8085.133	13508.16	6457.777	10298.76	4187.15	2467.345
ZnO	12569.97	9525.438	13643.69	7491.974	6457.777	14990.85	8918.528	8598.128	2571.629
ZrO_2	20614.53	16093.3	18854.16	12673.07	10298.76	8918.528	21837.61	10714.09	4265.301
Others	6075.249	9802.373	12974.22	7129.218	4187.15	8598.128	10714.09	29536.51	2622.814
T_0	5025.565	4281.325	5226.093	3029.404	2467.345	2571.629	4265.301	2622.814	1122.064

Table C 4. Variance-Covariance Matrix for w_{SO3} Model

Terms	Al_2O_3	B_2O_3	CaO	F	K_2O	Li_2O	Na_2O	P_2O_5
Al_2O_3	2.740819	-0.429431479	-1.89418	-0.53773	-0.14905	-0.26959	0.875313	-0.15096
B_2O_3	-0.42943	0.595220109	0.773142	0.124146	0.056482	-0.21059	-0.19365	-0.25499
CaO	-1.89418	0.773141748	9.593147	-0.67091	-0.35609	-1.2206	-1.32976	-1.09337
F	-0.53773	0.124145607	-0.67091	11.45471	0.163877	0.122649	0.076304	-2.18755
K_2O	-0.14905	0.056482102	-0.35609	0.163877	0.617562	0.017293	-0.02189	0.048654
Li_2O	-0.26959	-0.21059049	-1.2206	0.122649	0.017293	1.853893	0.403849	0.053591
Na_2O	0.875313	-0.193648887	-1.32976	0.076304	-0.02189	0.403849	0.53559	0.044177
P_2O_5	-0.15096	-0.254987221	-1.09337	-2.18755	0.048654	0.053591	0.044177	4.539892
SiO_2	-0.27555	-0.020791427	0.870288	-0.16677	-0.04449	-0.18058	-0.20274	-0.04626
V_2O_5	0.042695	-0.078302262	0.09155	-0.15828	-0.08491	-0.1464	-0.03646	0.101647
ZrO_2	0.125023	-0.000758407	-0.84636	-0.29043	-0.02152	-0.00957	0.008065	0.10608
Others	-0.13636	-0.006629682	-0.81139	0.230354	0.007898	-0.12297	-0.06201	0.032272
B_2O_3xCaO	4.529936	-7.387287771	-18.0109	4.530347	-0.51977	4.815481	3.334863	3.653491
Al_2O_3xNa_2O	-14.0724	1.565707935	7.914132	2.794817	0.901083	1.334898	-4.85952	0.614923
CaOxSiO_2	3.470327	-0.108355277	-20.3868	0.826639	1.196327	1.993506	2.52452	1.872637

Terms	SiO_2	V_2O_5	ZrO_2	Others	B_2O_3xCaO	Al_2O_3xNa_2O	CaOxSiO_2
Al_2O_3	-0.27555	0.042695	0.125023	-0.13636	4.529936	-14.0724	3.470327
B_2O_3	-0.02079	-0.0783	-0.00076	-0.00663	-7.38729	1.565708	-0.10836
CaO	0.870288	0.09155	-0.84636	-0.81139	-18.0109	7.914132	-20.3868
F	-0.16677	-0.15828	-0.29043	0.230354	4.530347	2.794817	0.826639
K_2O	-0.04449	-0.08491	-0.02152	0.007898	-0.51977	0.901083	1.196327
Li_2O	-0.18058	-0.1464	-0.00957	-0.12297	4.815481	1.334898	1.993506
Na_2O	-0.20274	-0.03646	0.008065	-0.06201	3.334863	-4.85952	2.52452
P_2O_5	-0.04626	0.101647	0.10608	0.032272	3.653491	0.614923	1.872637
SiO_2	0.143573	0.00159	-0.08547	-0.06059	-0.51998	1.421602	-2.20577
V_2O_5	0.00159	0.723663	0.066832	-0.02211	0.077115	0.129538	-0.35693
ZrO_2	-0.08547	0.066832	0.531451	0.106672	-0.09779	-0.30846	2.180157
Others	-0.06059	-0.02211	0.106672	0.340328	0.936866	0.978968	2.049753
B_2O_3xCaO	-0.51998	0.077115	-0.09779	0.936866	133.5691	-15.3203	13.79512
Al_2O_3xNa_2O	1.421602	0.129538	-0.30846	0.978968	-15.3203	77.91777	-14.7114
CaOxSiO_2	-2.20577	-0.35693	2.180157	2.049753	13.79512	-14.7114	50.36108

Table C 5. Variance-Covariance Matrix for K-3 Corrosion Model

Term	$S_{0/1}$	Al_2O_3	B_2O_3	CaO	Cr_2O_3	Fe_2O_3	Li_2O	MgO	MnO	Na_2O	P_2O_5
$S_{0/1}$	0.0115205	-0.0259845	0.0105021	-0.0055094	0.7912524	-0.022274	-0.0250001	0.1225018	0.0497994	0.0014595	-0.1198906
Al_2O_3	-0.0259845	0.9078704	-0.3848186	0.0655592	-0.3134741	0.3574367	-1.0937825	-1.3933142	-0.5690039	-0.4411739	-0.2909698
B_2O_3	0.0105021	-0.3848186	0.6333252	-0.0462628	-3.0899732	-0.2838156	0.187177	0.1119393	-0.1348884	0.0581645	-0.4864213
CaO	-0.0055094	0.0655592	-0.0462628	0.7520498	-6.6193434	0.5211735	-0.4234799	-7.3276124	1.201607	0.0649331	0.0829962
Cr_2O_3	0.7912524	-0.3134741	-3.0899732	-6.6193434	2278.8117	16.352916	-27.354499	-141.86608	47.389391	9.534999	-42.240184
Fe_2O_3	-0.022274	0.3574367	-0.2838156	0.5211735	16.352916	6.0716346	-1.5212947	-5.0624116	15.203711	-0.2856909	-1.0154266
Li_2O	-0.0250001	-1.0937825	0.187177	-0.4234799	-27.354499	-1.5212947	10.313724	-18.01376	-11.010525	2.756291	1.0641759
MgO	0.1225018	-1.3933142	0.1119393	-7.3276124	-141.86608	-5.0624116	-18.01376	559.43113	37.508813	-15.883733	13.823547
MnO	0.0497994	-0.5690039	-0.1348884	1.201607	47.389391	15.203711	-11.010525	37.508813	183.26939	-2.7798174	-2.2641063
Na_2O	0.0014595	-0.4411739	0.0581645	0.0649331	9.534999	-0.2856909	2.756291	-15.883733	-2.7798174	1.2724992	-0.1542709
P_2O_5	-0.1198906	-0.2909698	-0.4864213	0.0829962	-42.240184	-1.0154266	1.0641759	13.823547	-2.2641063	-0.1542709	21.30775
SiO_2	-0.0109881	0.1620387	-0.0802996	-0.1790029	-2.4103292	-0.0991283	-1.1142795	9.5458676	0.6981777	-0.5564337	0.0686619
SnO_2	0.0168227	0.35004	0.0519762	0.5821942	16.374784	1.7014239	-2.6638182	-8.4629113	6.5216847	-0.3624318	-0.3855029
TiO_2	-0.0108929	-0.097235	0.0335941	-0.7369181	21.436833	-2.8022463	-0.8377586	14.874823	5.9047782	0.8669899	2.104386
V_2O_5	0.008806	0.1899916	-0.0459042	0.3486891	-10.611306	1.9772128	-1.8054721	-18.262549	3.9586797	-0.2342114	-0.9349373
ZnO	0.1223421	-0.4893703	-0.1356733	-0.0637411	6.5681928	-0.1703298	0.2118988	4.4728865	6.6917421	0.2150816	1.248395
ZrO_2	0.0353666	0.0547449	-0.0465071	0.1772235	-5.4861406	0.5546621	-1.2039694	4.5140081	0.6732452	-0.6017456	1.0013744
Others	-0.0236834	0.0403552	-0.0050036	0.3026545	-19.752412	-0.7301265	2.0603601	-17.320408	-5.8257811	0.6476704	-0.2260611
$Fe_2O_3xFe_2O_3$	0.4648447	-3.7002902	3.2842755	-3.2099547	-188.24423	-64.755736	14.511424	19.918184	-257.69798	2.9258264	8.5148908
$Na_2OxCr_2O_3$	-3.5657541	-3.7102834	16.012474	28.874775	-10488.941	-70.083877	113.6031	862.26778	-207.66878	-54.781244	165.65563
TiO_2xNa_2O	0.0550441	0.0180735	0.903799	5.9488394	-184.13366	13.75992	3.0368881	-80.83336	-3.2109586	-4.9271047	-7.8326327
SiO_2xMgO	-0.1903851	2.6658411	-0.319306	17.957061	371.73167	9.4959158	41.501469	-1347.0592	-89.175223	38.899969	-34.958592
Term	SiO_2	SnO_2	TiO_2	V_2O_5	ZnO	ZrO_2	Others	$Fe_2O_3xFe_2O_3$	$Na_2OxCr_2O_3$	TiO_2xNa_2O	SiO_2xMgO
$S_0/1$	-0.0109881	0.0168227	-0.0108929	0.008806	0.1223421	0.0353666	-0.0236834	0.4648447	-3.5657541	0.0550441	-0.1903851
Al_2O_3	0.1620387	0.35004	-0.097235	0.1899916	-0.4893703	0.0547449	0.0403552	-3.7002902	-3.7102834	0.0180735	2.6658411
B_2O_3	-0.0802996	0.0519762	0.0335941	-0.0459042	-0.1356733	-0.0465071	-0.0050036	3.2842755	16.012474	0.903799	-0.319306
CaO	-0.1790029	0.5821942	-0.7369181	0.3486891	-0.0637411	0.1772235	0.3026545	-3.2099547	28.874775	5.9488394	17.957061
Cr_2O_3	-2.4103292	16.374784	21.436833	-10.611306	6.5681928	-5.4861406	-19.752412	-188.24423	-10488.941	-184.13366	371.73167
Fe_2O_3	-0.0991283	1.7014239	-2.8022463	1.9772128	-0.1703298	0.5546621	-0.7301265	-64.755736	-70.083877	13.75992	9.4959158
Li_2O	-1.1142795	-2.6638182	-0.8377586	-1.8054721	0.2118988	-1.2039694	2.0603601	14.511424	113.6031	3.0368881	41.501469
MgO	9.5458676	-8.4629113	14.874823	-18.262549	4.4728865	4.5140081	-17.320408	19.918184	862.26778	-80.83336	-1347.0592
MnO	0.6981777	6.5216847	5.9047782	3.9586797	6.6917421	0.6732452	-5.8257811	-257.69798	-207.66878	-3.2109586	-89.175223
Na_2O	-0.5564337	-0.3624318	0.8669899	-0.2342114	0.2150816	-0.6017456	0.6476704	2.9258264	-54.781244	-4.9271047	38.899969
P_2O_5	0.0686619	-0.3855029	2.104386	-0.9349373	1.248395	1.0013744	-0.2260611	8.5148908	165.65563	-7.8326327	-34.958592
SiO_2	0.3416855	0.006907	-0.0648293	-0.1870498	-0.318042	0.0571712	-0.3875321	-0.1171078	15.74098	-0.1322433	-23.396165
SnO_2	0.006907	6.4875366	-1.0995965	1.2479217	0.7627724	-0.654561	-0.9946303	-13.269812	-120.77706	6.5763137	18.727675
TiO_2	-0.0648293	-1.0995965	59.486296	-1.5267646	0.46586	0.4910005	-1.6500481	13.332777	-130.41662	-264.73203	-53.13404

V_2O_5	-0.1870498	1.2479217	-1.5267646	5.08211	0.1978155	0.536722	0.2490385	-14.173047	48.221925	10.112044	43.935411
ZnO	-0.318042	0.7627724	0.46586	0.1978155	5.6194942	-0.2622785	-0.3318092	0.146232	-38.962095	-1.8070845	-13.538345
ZrO_2	0.0571712	-0.654561	0.4910005	0.536722	-0.2622785	2.3514577	-0.1757394	-0.408651	24.349535	-2.4848846	-11.347441
Others	-0.3875321	-0.9946303	-1.6500481	0.2490385	-0.3318092	-0.1757394	2.1593925	6.8409854	83.582641	8.0778918	41.597185
$Fe_2O_3xFe_2O_3$	-0.1171078	-13.269812	13.332777	-14.173047	0.146232	-0.408651	6.8409854	858.90555	836.48141	-79.93767	-21.832643
$Na_2OxCr_2O_3$	15.74098	-120.77706	-130.41662	48.221925	-38.962095	24.349535	83.582641	836.48141	50585.519	1117.5022	-2165.6589
TiO_2xNa_2O	-0.1322433	6.5763137	-264.73203	10.112044	-1.8070845	-2.4848846	8.0778918	-79.93767	1117.5022	1266.4662	265.20753
SiO_2xMgO	-23.396165	18.727675	-53.13404	43.935411	-13.538345	-11.347441	41.597185	-21.832643	-2165.6589	265.20753	3291.0587

Table C 6. Variance-Covariance Matrix for Phosphate Model

Term	CaO	Li_2O	Na_2O	P_2O_5	SiO_2	RE_2O_3	Others	SiO_2xNa_2O
CaO	112.57	-95.62	156.36	33.574	51.402	204.63	-34.93	-560.2
Li_2O	-95.62	317.07	-224.7	-88.66	-84.19	42.313	29.193	1007.2
Na_2O	156.36	-224.7	1205.5	23.631	290.26	207.73	-165	-4133
P_2O_5	33.574	-88.66	23.631	187	17.347	-449.1	-5.039	-286.4
SiO_2	51.402	-84.19	290.26	17.347	83.74	12.801	-45.21	-1050
RE_2O_3	204.63	42.313	207.73	-449.1	12.801	7108.4	-63.43	-62.27
Others	-34.93	29.193	-165.0	-5.039	-45.21	-63.43	28.076	564.33
SiO_2xNa_2O	-560.2	1007.2	-4133	-286.4	-1050	-62.27	564.33	14696

Appendix D - Glass Forming Chemical Compositions

Table D 1. Nominal GFC composition in mass fractions

Oxide	Kyanite	Boric acid	Wollastonite	Na_2CO_3	Li_2CO_3	Cr_2O_3	Silica	Zincite	Zircon	V_2O_5
Al_2O_3	0.570223	0	0.002003	0	0	0	0.001657	0	0.002502	0
B_2O_3	0	0.565221	0	0	0	0	0	0	0	0
CaO	0.000267	0	0.475099	1.29×10^{-5}	0.003657	0	0.0001	0	0	0
CdO	0	0	0	0	0	0	0	0.0001	0	0
Cl	0	0	0	0.000174	8.32×10^{-5}	0	0	0	0	0
Cr_2O_3	0	0	0	7.77×10^{-5}	0.0001	0.990223	0	0	0	0
Fe_2O_3	0.007568	0	0.004003	1.3×10^{-5}	1.67×10^{-5}	3.88×10^{-5}	0.000217	1.66×10^{-5}	0.000783	0.000074
K_2O	0.000116	0	0	0	1.66×10^{-5}	0	3.35×10^{-5}	0	0	2.34×10^{-5}
Li_2O	0	0	0	0	0.402062	0	0	0	0	0
MgO	0.000133	0	0.000835	1.3×10^{-5}	9.99×10^{-5}	0	8.33×10^{-5}	0	0	0
MnO	0	0	0.001	0	0	0	0	1.66×10^{-5}	0	0
Na_2O	0.003495	0	0	0.58376	0.000716	0	0.000167	0	0	4.36×10^{-5}
NiO	0	0	0	0	0	0	0	0	0	0
P_2O_5	0	0	0	0	0	0	0	0	0	0
PbO	0	0	0	0	0	0	0	1.66×10^{-5}	0	0
SO_3	0	4.98×10^{-5}	0	0.0001	0.000266	0	0	0	0	0
SiO_2	0.406079	0	0.508207	0	0	0	0.996506	0	0.322526	2.77×10^{-5}
TiO_2	0.008769	0	0.0002	0	0	0	0.00015	0	0.001017	0
UO_3	0	0	0	0	0	0	0	0	0.00045	0
V_2O_5	0	0	0	0	0	0	0	0	0	0.994
ZnO	0	0	0	0	0	0	0	0.998145	0	0
ZrO_2	0	0	0	0	0	0	0	0	0.660036	0

Pacific Northwest National Laboratory

902 Battelle Boulevard
P.O. Box 999
Richland, WA 99354

1-888-375-PNNL (7665)

www.pnnl.gov